Deltares

# Ten Noorden van de Waddeneilanden Field Measurement Campaign

## Validation Report - February 2020

Deltares

# Ten Noorden van de Waddeneilanden Field Measurement Campaign

**Validation Report - February 2020**

Sofia Caires

11203488

Deltares

**Title**
Ten Noorden van de Waddeneilanden Field Measurement Campaign

| Client | Project | Reference | Pages |
|---|---|---|---|
| Fugro | 11203488 | 11203488-002-HYE-0002 | 41 |

**Classification**
None

**Keywords**
North Sea, wind farm, metocean data, validation, offshore wind

**Summary**

Two *SEAWATCH Wind LiDAR Buoys*, TNWA and TNWB, and a bottom mounted sensor associated to TNWB have been deployed by Fugro at the Ten Noorden van de Waddeneilanden Wind Farm Zone on the 19th of June 2019, with the intention of measuring wind, waves, temperatures, pressures and currents for a period of two years. This report focuses on the validation of the measurements during February 2020.

Because the LiDARs on both buoys stopped working at the end of December, on the 22nd of January both buoys were recovered and another buoy deployed at TNWA. However, due to the weather conditions it was not possible to place a buoy at TNWB before the end of February 2020. Consequently, there are no data from TNWB for the whole February 2020. On the other hand, the availability of the data from the TNWA buoy is high for all instruments, except for the LiDAR, which is acceptable, and the air temperature sensor, which is poor.

The validation is performed by comparing the TNWA observations against with wind, waves, air and water temperature, air pressure and currents from a variety of reliable sources (anemometer, LiDAR, hydrodynamic model, etc) at reference stations in the North Sea; namely L91, F161, K13, F3, AWG, HG, SON and BG.

The following conclusions ensue from the validation of the TNWA data.

- There is a good to excellent agreement between the wind observations from TNWA and those from the fixed platforms. Given that the found mismatches can be explained by local effects and spatial variations, it can be concluded that the accuracy of the TNWA wind speeds and directions is high.

- The agreement between the wave observations from TNWA and from the reference stations is relatively high, especially when considering local effects and the discreteness of the wave spectra.

- The validation of the water temperature data shows large spatial variations, leading to poor agreements between the data. On the other hand, there is a good agreement between the TNWA observed air temperatures and those from the nearby BG station.

- The validation of the air pressure data shows that in spite of a spatial gradient, given their proximity in terms of macro-atmospheric forcings, there is an excellent agreement between the TNWA observations and those from the fixed stations.

- The agreement between the current speed observations and model results is high. There are mismatches between the current directions, which are partly due to the nature and variability of the current direction signal.

The overall conclusion of the validation is that the TNWA dataset is of high quality and trustworthy.

**References**

None

| Version | Date | Author | Initials | Review | Initials | Approval | Initials |
|---|---|---|---|---|---|---|---|
| 4.0 | Apr 20, 2020 | S. Caires |  | J. Schouten |  | M. van Gent |  |

**Status**

Final

Deltares

# Contents

Deltares

## List of Figures

# List of Tables

# 1 Introduction

Aiming at high collection rates of quality metocean data, two *SEAWATCH Wind LiDAR Buoys* were deployed by Fugro at the Ten Noorden van de Waddeneilanden Wind Farm Zone. The two buoys are referred to as Station A and Station B but are abbreviated in this report as TNWA and TNWB, respectively. Additionally, a bottom mounted water level sensor (WLS) has been deployed near the TNWB buoy[1]. The deployment date is the 19$^{th}$ of June 2019. The campaign aims at measuring wind, waves, temperatures, pressures and currents for a period of two years and the redundant arrangement of instruments is intended to safeguard against loss in measured data. Unfortunately, because the LiDARs in both buoys stopped working, on the 22$^{nd}$ of January buoy WS190 was swapped with buoy WS170 at TNWA and buoy WS191 removed and not yet re-deployed nor replaced. Also, there is since then no data available from the WLS that has been deployed close to the TNWB buoy mooring location at the start of the campaign.

Information regarding the locations of the TNWA buoy is given in Table 1.1. The bathymetry around the location of the TNWA buoy and previous location of the TNWB buoy is shown in Figure 1.1.

***Table 1.1:*** *Ten Noorden van de Waddeneilanden Station A mooring location.*

| Station | S.no. | Longitude (E) | Latitude (N) | Depth (mMSL) |
|---|---|---|---|---|
| TNWA | WS170 | 5.5502° | 54.0181° | ≈ 38 |

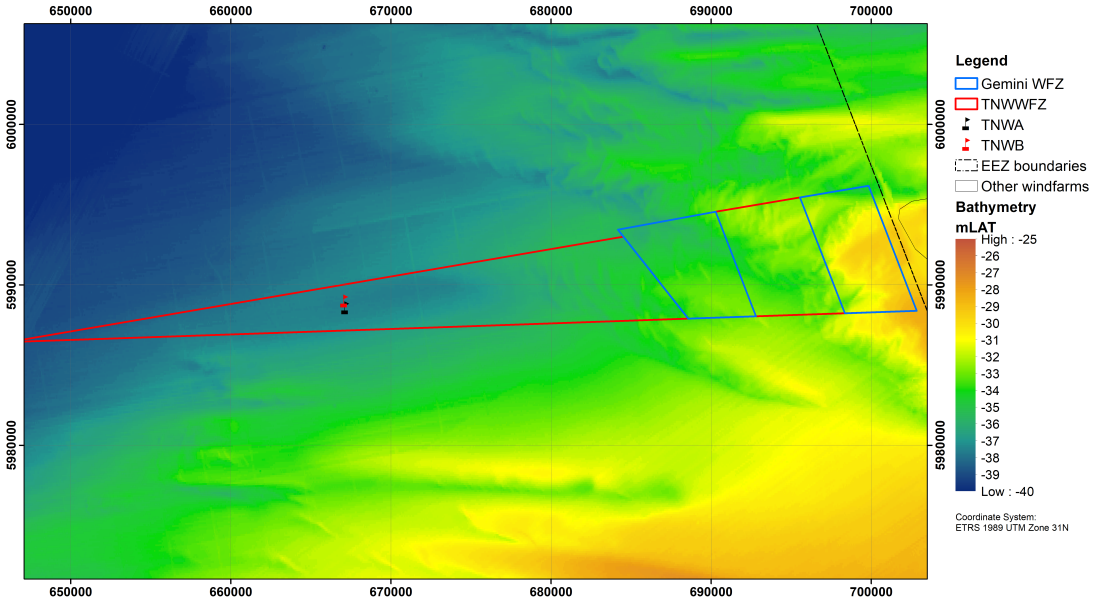


***Figure 1.1:*** *Bathymetry (mLAT, mLAT≈ -1 mMSL) around the buoy locations.*

The main aim of this report is to provide an overview and validation of the TNWA post-processed wind, wave, temperature, air pressure and current observations, mainly focusing on the validation of the wind, wave and current data. The assessment of the

[1] A WLS was also deployed near the TNWA buoy but it failed right after deployment.

integrity of the buoy data processing and the quality of the pre-processed data are outside the scope of the validation. The validation is carried out by quantifying the agreement between the TNWA data and data from other reliable sources (anemometer, LiDAR, atmospheric model, hydrodynamic model, etc) at fixed North Sea reference stations (no temporary campaigns). If the same variations are found in the parameters, this can be seen as an indication that the buoy systems are functioning correctly with no system errors in the measurements. Furthermore, for some variables their general characteristics are also qualitatively assessed, such as for current and wind measurements their respective vertical profiles. Per variable the most suitable available data validation sources have been sought, leading to the following combinations:

- The reference stations for validating the buoy wind data against anemometer observations are those from platform L91 (where the anemometer is at height z=87 m), referred to as L91, platform F161 (z=75.5 m), referred to as F161, platform K13 (z=73.8 m), referred to as K13, platform F3 (z=60 m), referred to as F3, platform Ameland Westgat (z=60 m), referred to as AWG and those from the Huibergat station (z=18 m), referred to as HG. These stations are approximately at a distance of respectively 59 km (L91), 101 km (F161), 178 km (K13), 107 km (F3), 64 km (AWG) and 75 km (HG) from the TNWA buoy. F161, K13 and F3 are thus at a considerable distance from TNWA and TNWB and the comparisons between these data can be expected to be poor. These data are still considered to provide a measure of spatial variability. The considered anemometer observations, as most other observations considered in this study, have been collected by the Dutch Government (see http://matroos.rws.nl/). LiDAR wind velocity observations at vertical levels 63 m, 91 m, 116 m, 141 m, 166 m, 191 m and 241 m at K13 from the Energy research Centre of the Netherlands (ECN) part of the Dutch organization for applied research (TNO) have also been made available and are also considered in the validation of the wind data. Furthermore, winds at 10 m height from the Dutch Meteorological Institute (KNMI) operational Numerical Weather Prediction model Hirlam7.2 (KNMI, 2009) are also considered in the evaluation of the spatial variations.
- The wave heights, periods and directions are also validated against Dutch Government observations. The locations for validating the buoy wave data are F161, F3 and Schiermonnikoog Noord, referred to as SON and at about 62 km from the TNWA buoy.
- The Dutch Government observations at K13 and SON are used for validating the water temperature.
- Available online data ( https://mesonet.agron.iastate.edu/request/download.phtml?network=NL__ASOS) from weather stations located at Buitengaats, referred to as BG and located within the TNW region, are used for validating the air temperature.
- Dutch Government observations at K13, F3, F161 and L91 are used for validating air pressure.
- Lastly, given the lack of fixed observation sources, the currents are validated against predictions from a purposely run by Deltares 3D hydrodynamic model.

Figure 1.2 shows an overview of all measurement locations. The present report provides the validation results for the period - 'February 2020' - extending from February 01 00:00 to February 29 23:50.

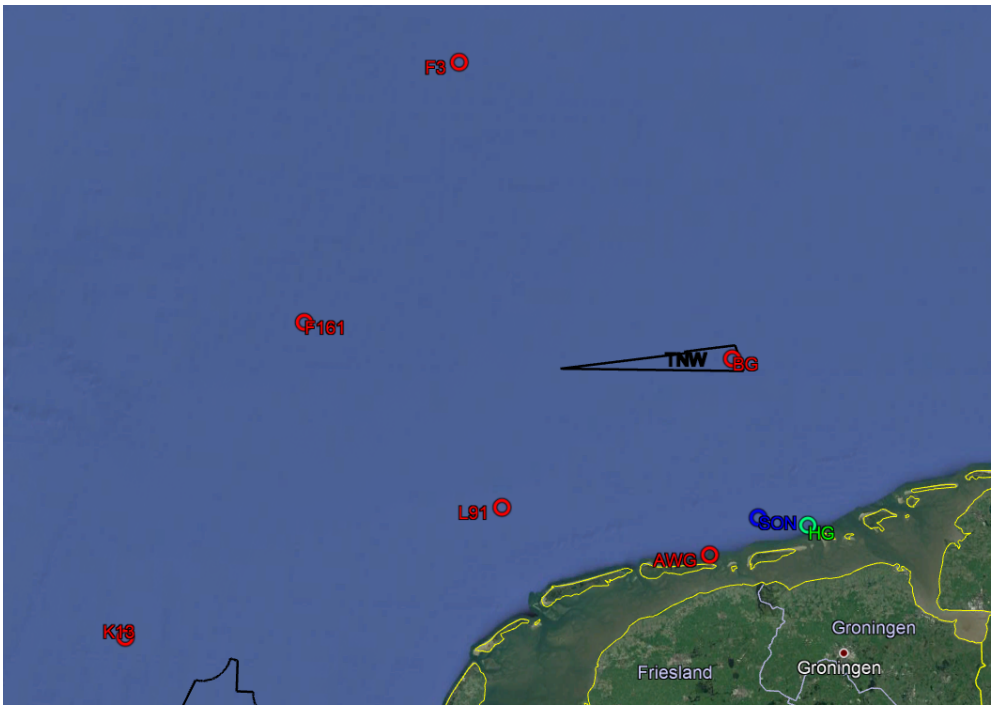


***Figure 1.2:*** *Aerial view of the location of the buoys and fixed measurement stations (via Google Earth).*

All comparisons are presented as a timeseries and further validated via direct scatter plots for quantifying statistical correspondence between the datasets.

The error statistics are computed differently whether a linear or circular (directional) variable is considered. For linear variables we have:

- the bias: $\bar{y} - \bar{x}$;
- the root-mean-square error: rmse = $\sqrt{n^{-1} \sum (y_i - x_i)^2}$;
- the symmetric slope: s = $\sqrt{\sum {x_i}^2 / \sum {y_i}^2}$; and
- the correlation coefficient:

$$r = \sum \left[ (x_i - \bar{x}) (y_i - \bar{y}) \right] / \sqrt{\sum (x_i - \bar{x})^2 \sum (y_i - \bar{y})^2} \, .$$

In all these formulae $x_i$ usually represents observations (or the dataset which is considered less uncertain or baseline) and in this study we use it to represent the fixed observations, $y_i$ usually represents the model results (or the dataset which is considered more uncertain or with a certain deviation from the baseline results) and in this study we use it to represent the TNWA or TNWB data and $n$ the number of observations.

When dealing with circular data, each observation is considered as unit vector, and it requires vector addition rather than ordinary (or scalar) addition to compute the average of angles, the so-called mean direction.

Writing

$$C_n = \sum_{i=1}^{n} \cos x_i \quad and \quad S_n = \sum_{i=1}^{n} \sin x_i, \tag{1.1}$$

the sample resultant vector $R_n$ of a sample $\mathbf{x} = x_i,\ i = 1, ..., n$ is defined as $R_n = \sqrt{C_n^2 + S_n^2}$, and its sample mean direction $\bar{x} \equiv \bar{x}_n$ as the direction of $R_n$:

$$\bar{x} = TAN^{-1}(S_n/C_n\ )$$

where

$$TAN^{-1}(S_n/C_n\ )$$

is the inverse of the tangent of

$$(S_n/C_n\ )$$

in the range [0, $2\pi$], i.e.,

$$TAN^{-1}(S_n/C_n\ ) := \begin{cases} \tan^{-1}(S_n/C_n\ ), & S_n > 0, \quad C_n > 0 \\ \tan^{-1}(S_n/C_n\ ) + \pi, & C_n < 0 \\ \tan^{-1}(S_n/C_n\ ) + 2\pi, & S_n < 0, \quad C_n > 0. \end{cases} \tag{1.2}$$

The sample mean resultant length of $\mathbf{x} = x_i,\ i = 1, ..., n$ is defined by $\bar{R}_n = R_n/n$ , $0 \leq \bar{R}_n \leq 1$. If $\bar{R}_n = 1$, then all angles coincide.

Equation 1.2 can be used to compute the bias between two circular variables by substituting $x_i$ by $y_i - x_i$ in Equation 1.1. In a similar way, the root-mean-square error between two circular variables can be computed.

There are several circular analogues of the correlation coefficient, but the most widely used is the so-called T-linear correlation coefficient (Fisher and Lee (1983) and Fisher (1993)). Given two sets $\mathbf{x} = x_i,\ i = 1, ..., n$, $\mathbf{y} = y_i,\ i = 1, ..., n$ of circular data, the T-linear correlation coefficient between x and y is defined by

$$r = \frac{\sum_{1 \leq i < j \leq n} \sin(x_i - x_j) \sin(y_i - y_j)}{\sqrt{\sum_{1 \leq i < j \leq n} \sin^2(x_i - x_j) \sum_{1 \leq i < j \leq n} \sin^2(y_i - y_j)}}. \tag{1.3}$$

In the following we shall refer to comparisons in which $r$ is higher than 0.9 as excellent, between 0.8 and 0.9 as good, between 0.7 and 0.8 as reasonable and lower than 0.7 as poor. Note that this is no absolute quality statement given that there are uncertainties in both observations and, due to the distance between the instruments, the spatial variability is expected to affect the comparisons.

Note that all reported dates are in GMT (which is equivalent to UTC).

## 1.1 Outline of the report

The availability of the considered TNWA data is given in the next chapter, followed by the description and validation of the wind, wave, temperature, pressure and current data in separate chapters. A summary of the drawn conclusions is given in the executive summary at the start of this report.

# 2 Data Availability

Although in measuring campaigns the aim is always of having a full (gap free) timeseries of all measured parameters, they are typically hampered by severe metocean conditions and loss of signal between instruments.

Figure 2.1 shows for each buoy and per parameter a detailed breakdown of the amount of missing data from February 01 00:00 to February 29 23:50. Table 2.1 gives a brief explanation of what the variable names in Figure 2.1 mean, their units and, if applicable, the symbols used to refer to them.

We note that in this validation study only processed data (10 minute averages in the case of wind) are considered. The original raw observations have been processed and quality checked by Fugro. When there are no gaps, the data from all processed variables are available every 10 minutes (at the hour and 10, 20 30, 40 and 50 minutes after the hour). As can be seen in Figure 2.1, the considered collected data consists of wind speed and direction at different heights, a number of wave height, period and direction parameters, current speed and direction at different depths, water and air temperature, pressure and humidity. We note further that not all data being measured (and processed by Fugro) are considered in this report:

- Although the availability of the humidity data is given in Figure 2.1, the data are not considered further.
- The WLS is also recording the water pressure, but these data are also not being considered, at least for the time being. After the collection of six months of water pressure data Fugro will check whether the data can be used to infer water levels.
- The buoys are also recording the wave spectra, but it is not transmitted on an ongoing basis. They will only be available every 6 months or so, after service visits when all data are downloaded.

As can also be seen in Figure 2.1, there are no data from TNWB available during this period. This is because the LiDARs on both buoys stopped working at the end of December and the buoys recovered for servicing on the 22$^{nd}$ of January. Although, buoy WS170 was then deployed at TNWA, due to the weather conditions it was not possible to place a buoy at TNWB before the end of February 2020.

We use the following qualification of data availability:

- >95% referred to as high availability,
- 90 - 95% referred to as good availability,
- 80 - 90% referred to as acceptable availability,
- 60 - 80% referred to as limited availability, and
- <60% referred to as poor availability.

According, the availability of the data from the TNWA buoy is high for all instruments, except for the LiDAR, which is acceptable, and the air temperature sensor, which is poor.

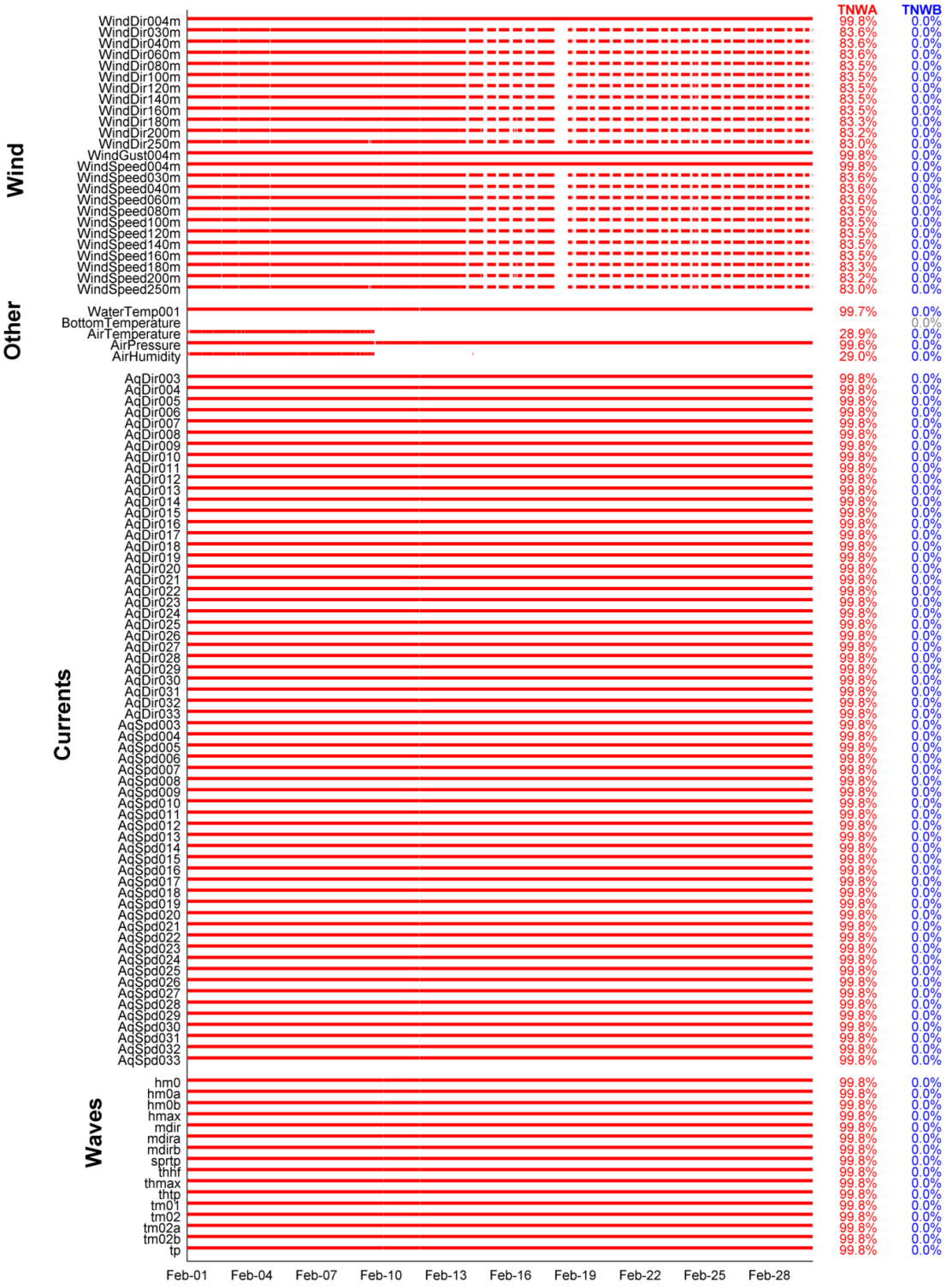


***Figure 2.1:*** *Availability of the 10 minute TNWA (red), TNWB (blue) and WLS (grey) data of February 2020.*

***Table 2.1:*** *List of variables.*

| Name | Description | Units | Symbol |
|---|---|---|---|
| WindSpeed $z$ mh | Wind speed at an elevation of $z$ m above the sea surface | m/s | $U_z$ |
| WindGust $z$ mh | Wind gust speed at an elevation of $z$ m above the sea surface | m/s | |
| WindDir $z$ m | Wind direction at an elevation of $z$ m above the sea surface | °N | $U_{z\theta}$ |
| airTemperature | Air temperature | °C | $T_{air}$ |
| airPressure | Air pressure | hPa | |
| airHumidity | Air humidity | % | |
| WaterTemp0001 | Water temperature (surface) | °C | $T_{water}$ |
| BottomTemp | Water temperature (bottom) | °C | $T_{water}$ |
| AqSpd $d$ | Current speed at a depth of $d$ m below the sea surface | m/s | $u_d$ |
| AqDir $d$ | Current direction at a depth of $d$ m below the sea surface | °N | |
| hm0 | Spectral significant wave height | m | $H_s$ |
| hm0a | Spectral significant swell wave height. Frequency band between 0.04 and 0.10 Hz. | m | $H_{sswell}$ |
| hm0b | Spectral significant sea wave height. Frequency band between 0.10 and 0.50 Hz. | m | $H_{ssea}$ |
| hmax | Spectral maximal individual wave height | m | $H_{max}$ |
| mdir | Mean wave direction | °N | $MWD$ |
| mdira | Mean wave direction of swell | °N | $MWD_{swell}$ |
| mdirb | Mean wave direction of sea | °N | $MWD_{sea}$ |
| sprtp | Wave spreading at spectral peak period | ° | $DSPR$ |
| thhf | High frequency mean wave direction. Frequency band between 0.4 and 0.44 Hz. | °N | |
| thmax | Period of highest wave. | s | |
| thtp | Wave direction at spectral peak period. | °N | |
| tm0$x$ | Spectral mean absolute wave period (1 based on the 1st spectral moment, 2 based on the 2nd spectral moment, a swell, b sea) | s | $T_{m0x}$ |
| tp | Spectral peak wave period | s | $T_p$ |

# 3 Wind

This chapter focuses on the validation of the TNWA wind velocity observations. The wind speed and direction are measured at 4 m above water level by a Sonic wind sensor and at levels 30, 40, 60, 80, 100, 120, 140, 160, 180, 200 and 250 m above water level by a LiDAR. An overview of the TNWA wind data is given next, followed by a validation using observed and model data.

Given that for low wind speeds there is much scatter in the data and that these data are not relevant in the data analyses (profiles and error statistics), all observations for which the observed wind speeds are below 5 m/s are excluded. This threshold was chosen pragmatically, being in line with the work of Wieringa and Rijkoort (1983) and in line with other wind climate assessments of the Dutch meteorological institute and close to the 4 m/s threshold prescribed for the calibration of cup anemometers in the IEC 61400-12-1 standard.

## 3.1 Ten Noorden van de Waddeneilanden description

To get a full overview of the data a movie was created with the time evolution of vertical wind profiles at TNWA (see here). Figure 3.1 provides a compacter overview of the observed TNWA LiDAR data, showing all observed vertical profiles for which the wind speed is above 5 m/s (grey lines), the mean profile (red line) and a fitted power profile (blue line).

The power law profile is described by:

$$U(z) = U_{30}\left(\frac{z}{30}\right)^{\alpha}$$

where $U_{30}$ is the wind speed at 30m above the surface and $\alpha$ is the power-law constant. The fit given in Figure 3.1 has been obtained using least squares.

Figure 3.1 shows that the power law profile deviates slightly from the observed vertical wind profile, showing a higher (lower) increase with height up to (above) a height of about 150 m.

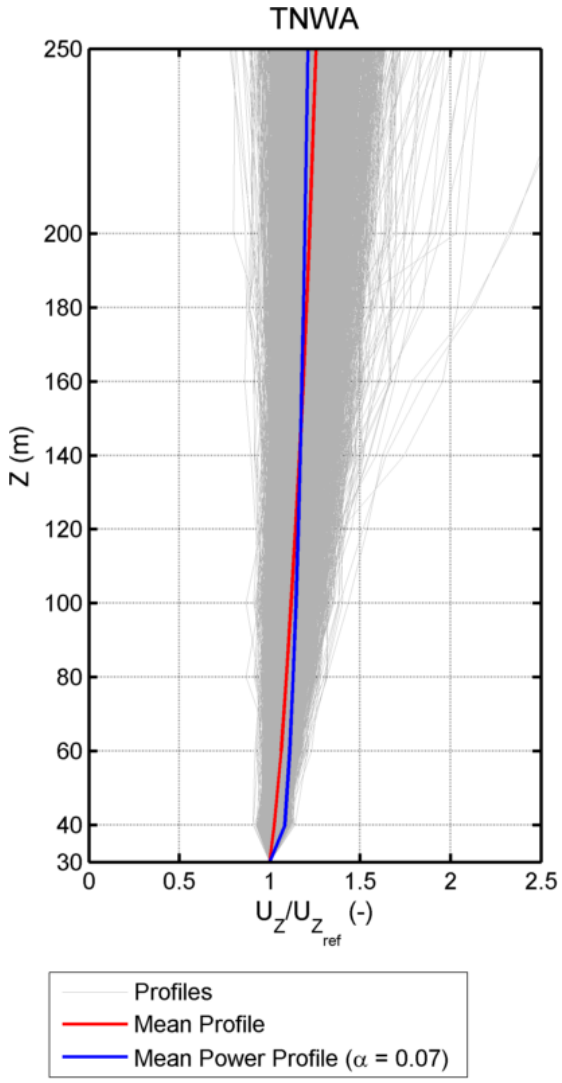


***Figure 3.1:*** *Normalized LiDAR wind speed vertical profiles (data from February 2020).*

Figure 3.2 shows the timeseries of the wind speed and direction at the observation levels. The figure shows that the period is characterized by two very heavy storms on the 9$^{th}$ (Ciara) and on the 16$^{th}$ (Dennis) of February, with observed wind speeds close to 40 m/s in the higher levels. During these storms the winds are from the Southwest and during the rest of the month predominantly from the West.

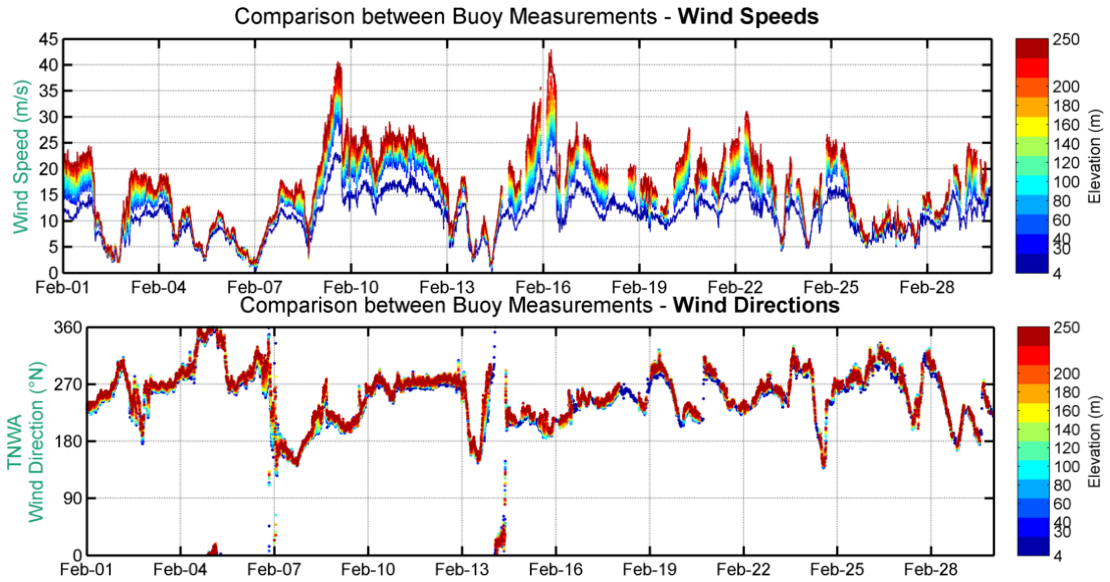


***Figure 3.2:*** *Wind speeds and directions (by elevation) at TNWA.*

## 3.2 Validation

In this section TNWA LiDAR wind velocities at a single level are validated against anemometer observations at L91 (at a height of z=87 m and at a distance of about d= 59 km from TNW), F161 (z=75.5 m, d=101 km), K13 (z=73.8 m, d=178 km), F3 (z=60 m, d=107 km), AWG (z=60 m, d=64 km), and HG (z=18 m, d=75 km). The wind speeds at several levels are validated against ECN LiDAR observations at K13 (z=63, 91, 116, 141, 166, 191 and 241 m). Note that F161, K13 and F3 are at a considerable distance from TNW and in periods with large spatial wind variations comparisons between these data can be expected to be poor. Furthermore, given its proximity to the coast, the winds blowing from the coast at HG and AWG are expected to be more strongly influenced by land effects. Nevertheless, data from these stations are still expected to show some correspondence with the TNWA data and in any case to provide a measure of spatial variability and also variability in height.

An overview of the comparisons between the TNWA and the fixed platform anemometer datasets is presented first, followed by a comparison of the TNWA data with measured fixed platform anemometer and LiDAR data. Finally, the spatial variability of the wind is evaluated using model data.

### 3.2.1 Overview

Figure 3.3 provides an overview of the comparisons, comparing the timeseries of the L91, F161, K13, F3, AWG, and HG observations and the TNWA LiDAR observations at the levels closer to those of the anemometers. (Note the outliers in the K13 observations, which have not been removed.) A further overview of the comparisons between data at the buoy and platform locations is given by means of wind roses in Figure 3.4. The roses show a general alignment between the datasets and that the most predominant winds during this period are from the West and the stronger winds from the Southwest. At L91 and F161 the western winds have a more southern direction. The rose for F3 is empty because there are no wind direction observations available during this period.

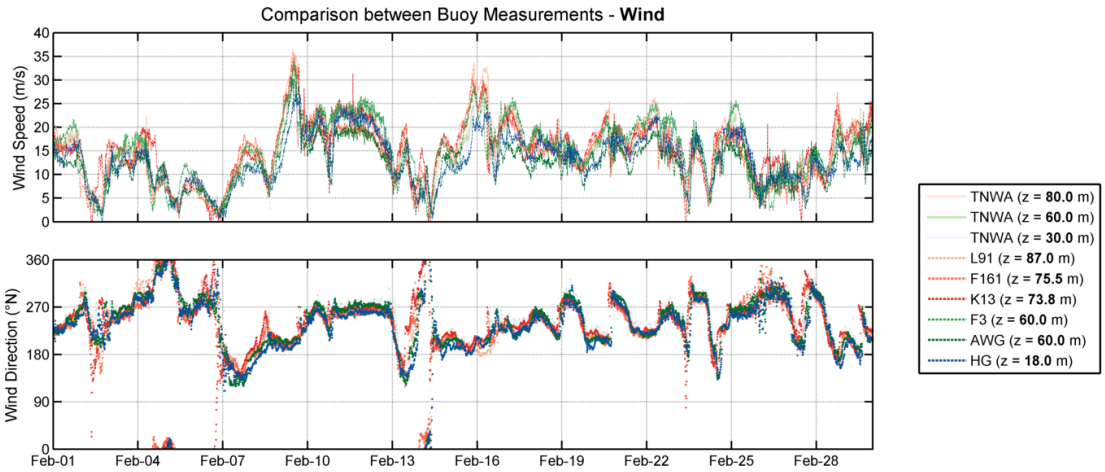


***Figure 3.3:*** *Wind speed and direction for all locations (data from February 2020).*

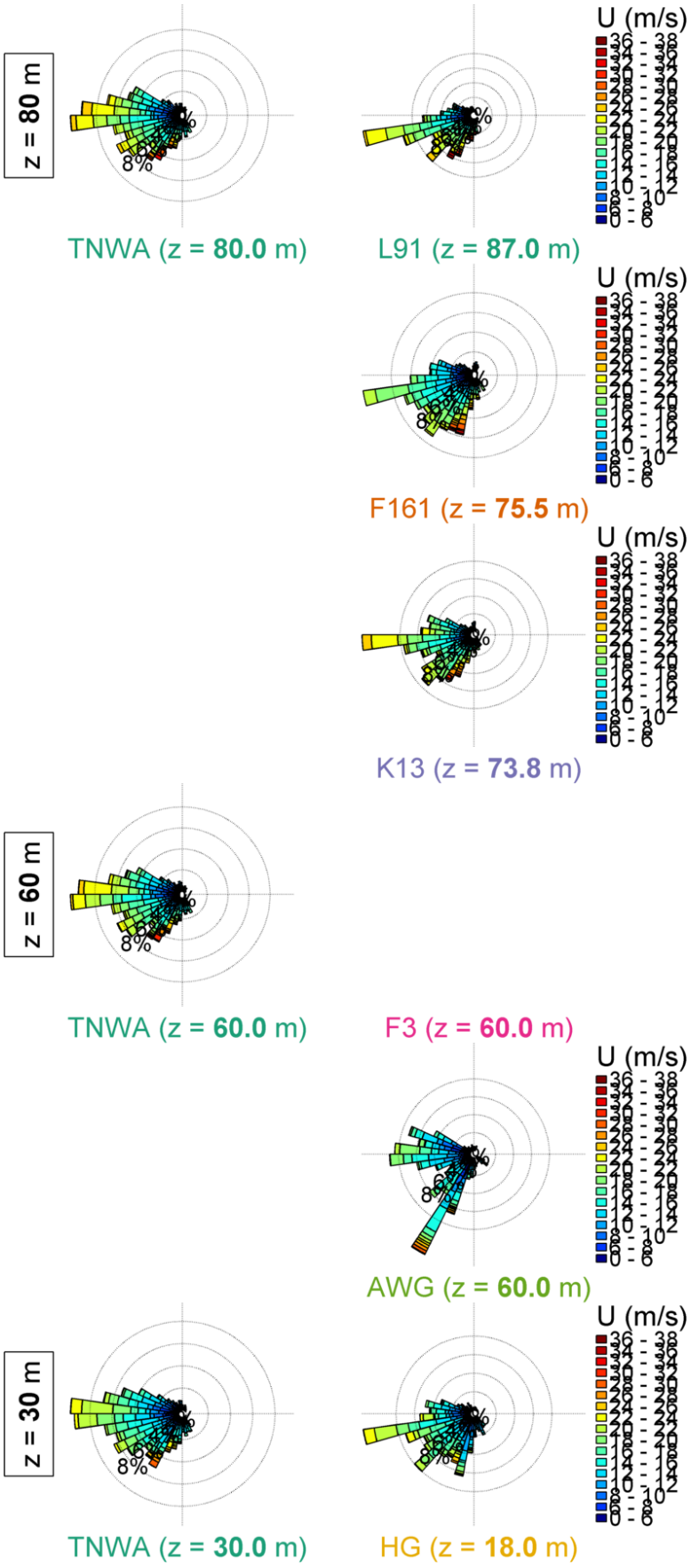


***Figure 3.4:*** *Wind roses (of bin width 8°) for all locations (data from February 2020).*

### 3.2.2 Comparisons

#### 3.2.2.1 Anemometer

Figure 3.5, Figure 3.6, Figure 3.7, Figure 3.8, Figure 3.9 and Figure 3.10 show comparisons between TNWA observations and those at L91, F161, K13, F3, AWG, and HG, respectively. The correlation, root-mean-square error and bias statistics are printed in the figures.

As can be seen in the figures, the comparisons between the TNWA observations and those from:

- L91 and HG are excellent in terms of both wind speed and direction,
- F161 and AWG are good in terms of wind speed and excellent in terms of wind direction,
- K13 are good in terms of both wind speed and direction, and
- F3 are good in terms of wind speed (there are no wind direction observations available).

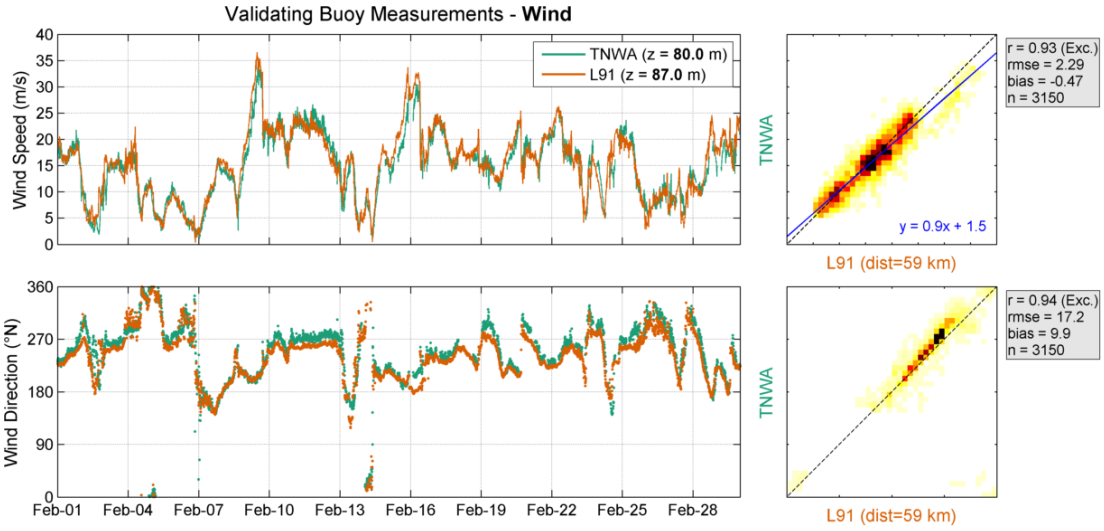


***Figure 3.5:*** *Validation of TNWA (data from February 2020) with L19 wind data. Left panel: Timeseries. Middle panel: Density scatter, with the darker colours indicating more data density.*

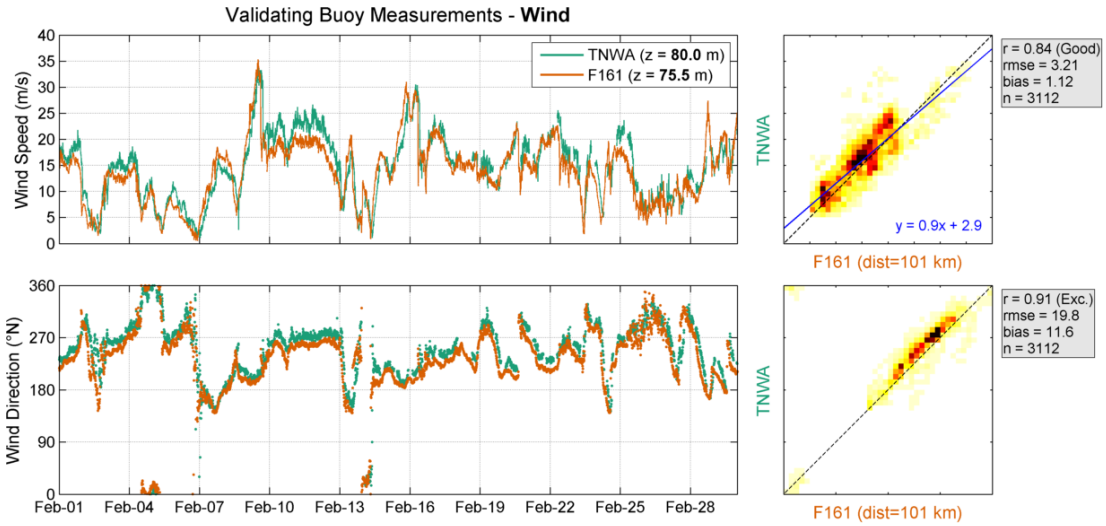


***Figure 3.6:*** *Validation of TNWA (data from February 2020) with F161 wind data. Left panel: Timeseries. Middle panel: Density scatter, with the darker colours indicating more data density.*

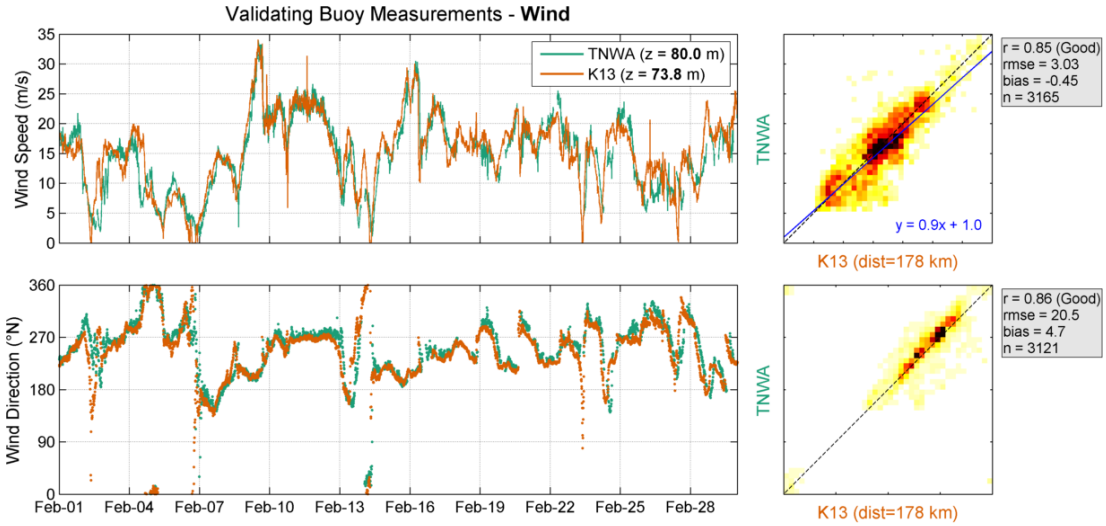


***Figure 3.7:*** *Validation of TNWA (data from February 2020) with K13 wind data. Left panel: Timeseries. Middle panel: Density scatter, with the darker colours indicating more data density.*

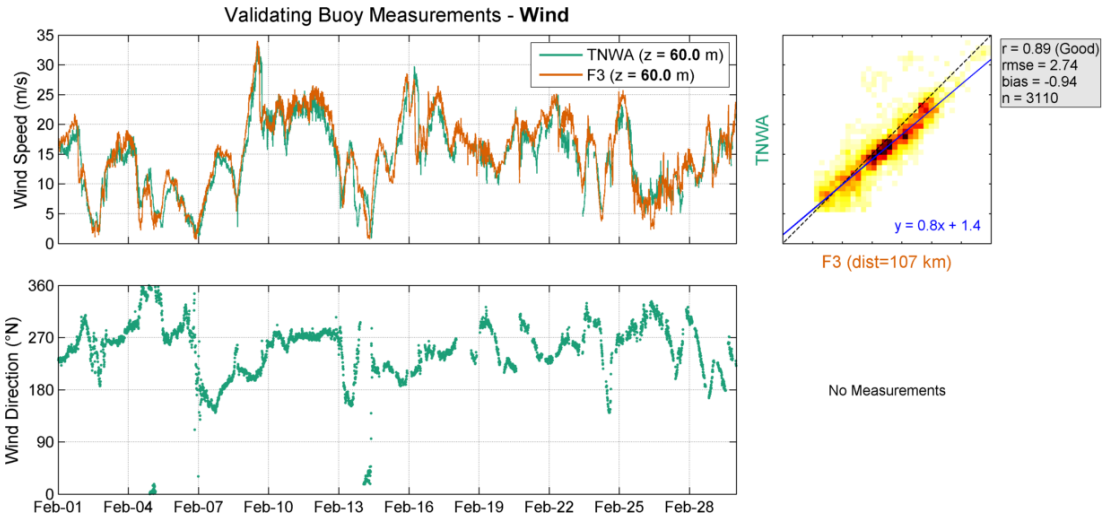


***Figure 3.8:*** *Validation of TNWA (data from February 2020) with F3 wind data. Left panel: Timeseries. Middle panel: Density scatter, with the darker colours indicating more data density.*

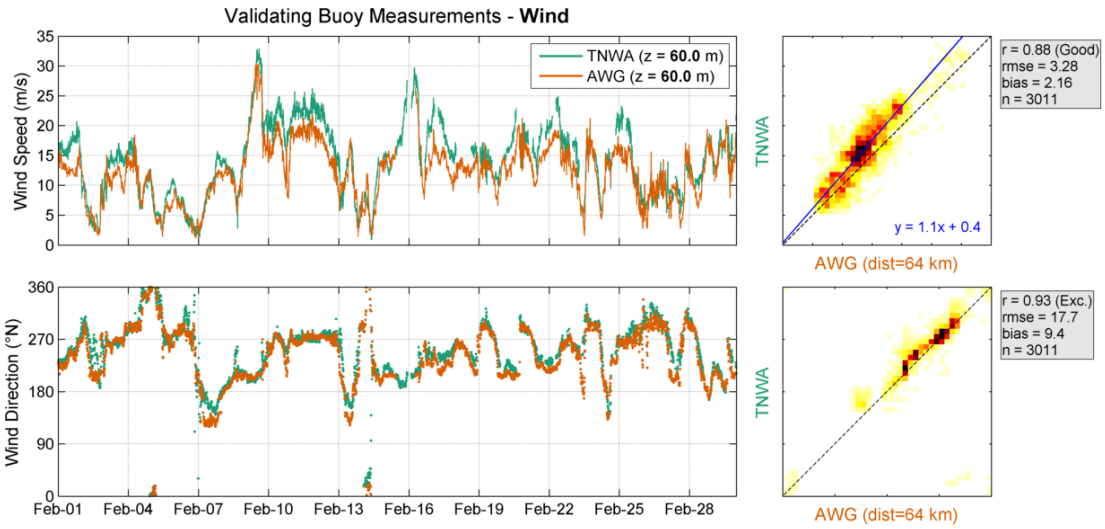


***Figure 3.9:*** *Validation of TNWA (data from February 2020) with AWG wind data. Left panel: Timeseries. Middle panel: Density scatter, with the darker colours indicating more data density.*

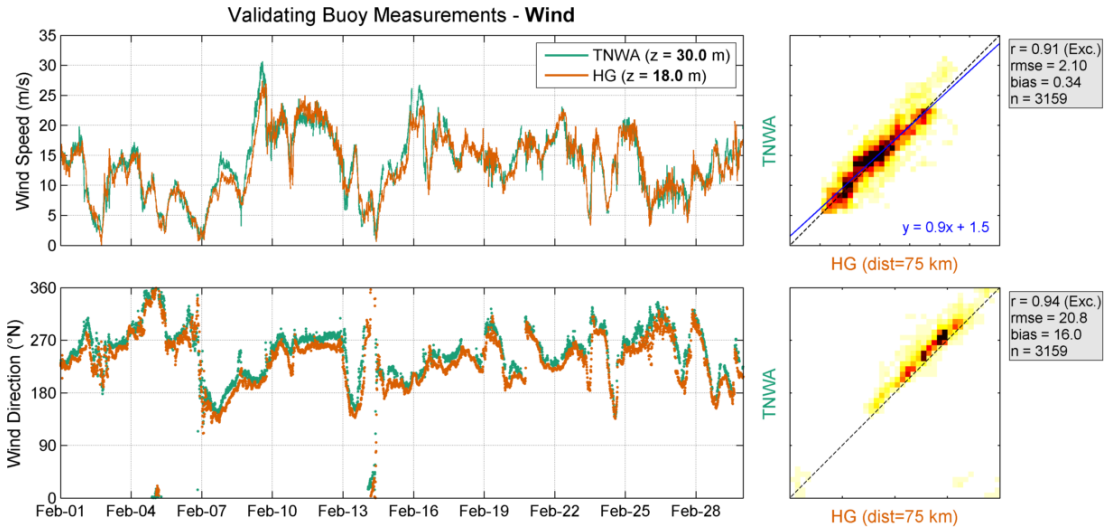


***Figure 3.10:*** *Validation of TNWA (data from February 2020) with HG wind data. Left panel: Timeseries. Middle panel: Density scatter, with the darker colours indicating more data density.*

### 3.2.2.2 LiDAR

In the following the TNWA wind data are compared with the LiDAR observations at K13. Before comparing the TNWA data with the K13 LiDAR data, these are validated against the anemometer data at K13. Figure 3.11 shows the comparison between the K13 LiDAR and anemometer timeseries. A timeseries comparison is provided (by elevation), with a density scatter comparing the best match (in terms of elevation) between the two datasets. I.e., the LiDAR measurements at the 63 m level are directly compared against the anemometer observations at the 73.8 m level. The correlations are excellent in terms of both wind speed and direction. As expected due to the difference in elevation (73.8 and 63 m), there is a bias in the wind speed, with the (observed at a higher height) anemometer wind speeds being on average higher.

Table 3.1 shows the comparisons between the TNWA observations and those of the closer vertical levels by the LiDAR at K13. As was also the case in the comparisons with the K13 anemometer, the comparisons are at all levels good in terms of both wind speed and direction.

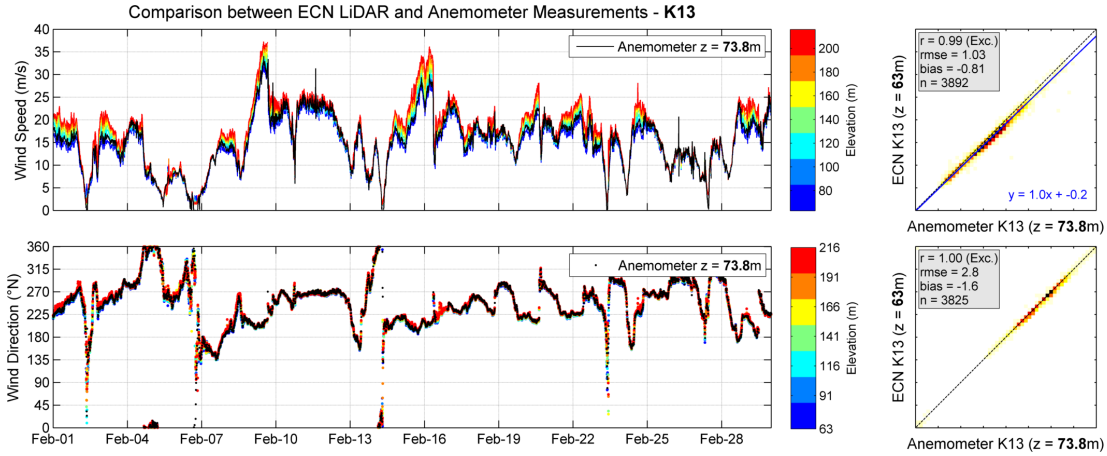


***Figure 3.11:*** *Comparison between ECN LiDAR and anemometer measurements at K13.*

***Table 3.1:*** *Statistical comparison between TNWA and K13 LiDARs at different heights.*

| Elevation | | Wind Speed | | | | Wind Direction | | |
|---|---|---|---|---|---|---|---|---|
| TNWA (m) | K13 (m) | $r$ (-) | Bias (m/s) | Symmetrical Slope (-) | $n$ (-) | $r$ (-) | Bias (°) | $n$ (-) |
| 60 | 63 | 0.84 | 0.11 | 1.00 | 3158 | 0.86 | -5.9 | 3158 |
| 100 | 91 | 0.85 | -0.04 | 0.99 | 3167 | 0.86 | -6.0 | 3167 |
| 120 | 116 | 0.85 | 0.13 | 1.00 | 3159 | 0.86 | -6.1 | 3159 |
| 140 | 141 | 0.85 | 0.21 | 1.00 | 3169 | 0.86 | -5.9 | 3169 |
| 160 | 166 | 0.85 | 0.28 | 1.01 | 3169 | 0.86 | -5.6 | 3169 |
| 200 | 191 | 0.85 | 0.07 | 0.99 | 3161 | 0.86 | -5.9 | 3161 |
| 250 | 241 | 0.86 | 0.03 | 0.99 | 3156 | 0.86 | -5.4 | 3156 |

### 3.2.3 Spatial and temporal variability

In order to further evaluate the spatial variations in the observation period, the wind fields from the Dutch Meteorological Institute (KNMI) operational Numerical Weather Prediction model Hirlam7.2 are also considered. The model fields are only available at 10 m and with an hourly resolution. The spatial resolution of the model is about 11 km x 11 km, which implies that the model in principle underestimates the spatial variations and coastal effects, i.e. the model results can be expected to be smoother than the true fields.

In order to characterize the most extreme event in the observation period, Figure 3.12 shows the model wind fields at the hour of the maximum observed 100 m wind speed at TNWA; at 14:00 on the 9th of July (the peak of storm Ciara, cf. Figure 3.2). The figure shows an extreme wind event from the Southwest, model 10 m wind speeds close to 27 m/s at all locations.

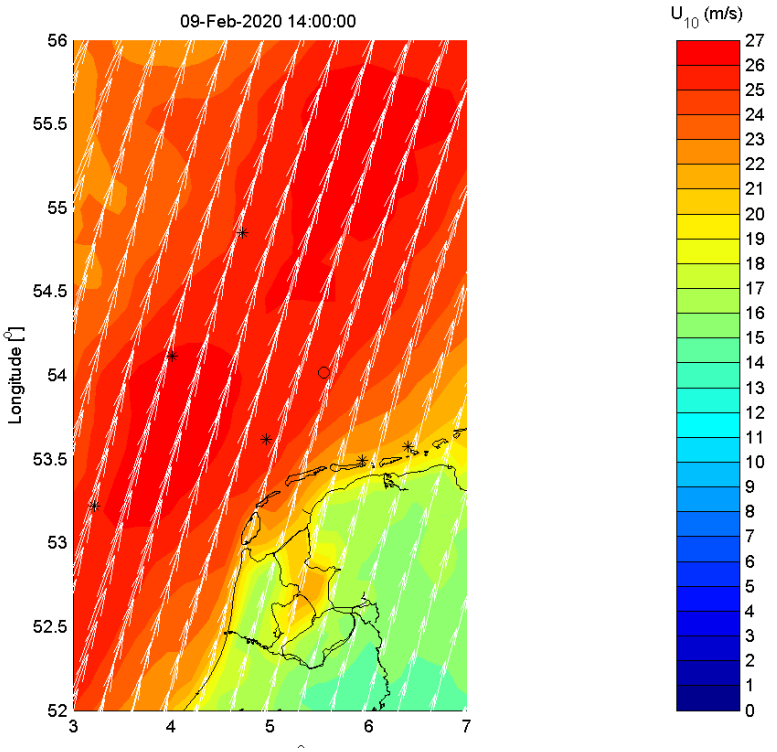


***Figure 3.12:*** *Hirlam7.2 wind field at the hour of the maximum TNWA 100 m wind speed. The *s indicate the locations of the fixed stations and the ○s the TNW locations.*

Table 3.2 shows the correlations between the Hirlam7.2 10 m (hourly) wind speeds and directions from the model grid points closer to TNWA and the fixed station locations at the timestamps at which the data from TNWA are valid. For these periods the corresponding correlations between the buoy and the fixed station anemometer (10 minute) observations (at the closer vertical levels) are given in figures 3.5 to 3.10 and reproduced Table 3.3. As can be seen in Table 3.2, the model winds at TNWA have the higher correlations with the winds at the L91 and AWG locations and the lowest with the winds at K13. The comparison of the correlations between the observations and the models results confirm that lower correlations are mostly due to spatial variations (note also the low correlations between the TNWA and K13 observations) and local effects (such as land effects at AWG and HG) which are less present in the model results due to its resolution.

***Table 3.2:*** *Statistical comparison between the model results at the TNWA buoy and at the fixed station locations at the timestamps at which the TNWA buoy data are valid*

| | **TNWA** | | |
|---|---|---|---|
| **Station** | $U_{10}$ $r$ **(-)** | $U_{dir}$ $r$ **(-)** | $n$ **(-)** |
| L91 | 0.97 | 0.97 | 546 |
| F161 | 0.94 | 0.94 | 546 |
| K13 | 0.86 | 0.87 | 546 |
| F3 | 0.95 | 0.96 | 546 |
| AWG | 0.96 | 0.97 | 546 |
| HG | 0.94 | 0.94 | 546 |

***Table 3.3:*** *Statistical comparison between the TNWA buoy observations and those from the fixed stations.*

| | **TNWA** | | | |
|---|---|---|---|---|
| **Station** | $U_{10}$ $r$ **(-)** | $n$ **(-)** | $U_{dir}$ $r$ **(-)** | $n$ **(-)** |
| L91 | 0.93 | 3150 | 0.94 | 3150 |
| F161 | 0.84 | 3112 | 0.91 | 3112 |
| K13 | 0.85 | 3165 | 0.86 | 3121 |
| F3 | 0.89 | 3110 | - | 0 |
| AWG | 0.88 | 3011 | 0.93 | 3011 |
| HG | 0.91 | 3159 | 0.94 | 3159 |

## 3.3 Conclusions

Based on the validation of the TNWA data against observations and model data, which shows that mismatches can be explained by local effects and spatial variations, it can be concluded that the accuracy of the TNWA wind speeds and directions is high.

# 4 Waves

The measured waves from TNWA are presented and analyzed within this chapter. The goal is to assess the reliability and accuracy of the retrieved TNWA wave data by means of a statistical validation against fixed wave measurements in the area.

## 4.1 Ten Noorden van de Waddeneilanden description

The timeseries of the main wave parameters observed at TNWA is shown in Figure 4.1. It includes the following parameters:

- significant wave height, $H_s$
- peak wave period, $T_p$
- mean wave direction, $MWD$
- swell and sea[1] significant wave heights, $H_{sswell}$ and $H_{ssea}$
- maximum wave height, $H_{max}$
- swell and sea mean wave directions, $MWD_{swell}$ and $MWD_{sea}$
- mean wave periods, $T_{m01}$ and $T_{m02}$, and
- swell and sea mean wave periods, $T_{m02swell}$ and $T_{m02sea}$.

During this period the waves are predominantly from the southwest to northwest quadrant and higher waves are from the Northwest. The highest observed waves are in the period between the 9th and the 12th of February.

[1] The swell and sea variables are computed from the spectral energy in the frequency band between respectively 0.04 and 0.10 Hz and 0.10 and 0.50 Hz (cf. Table 2.1).

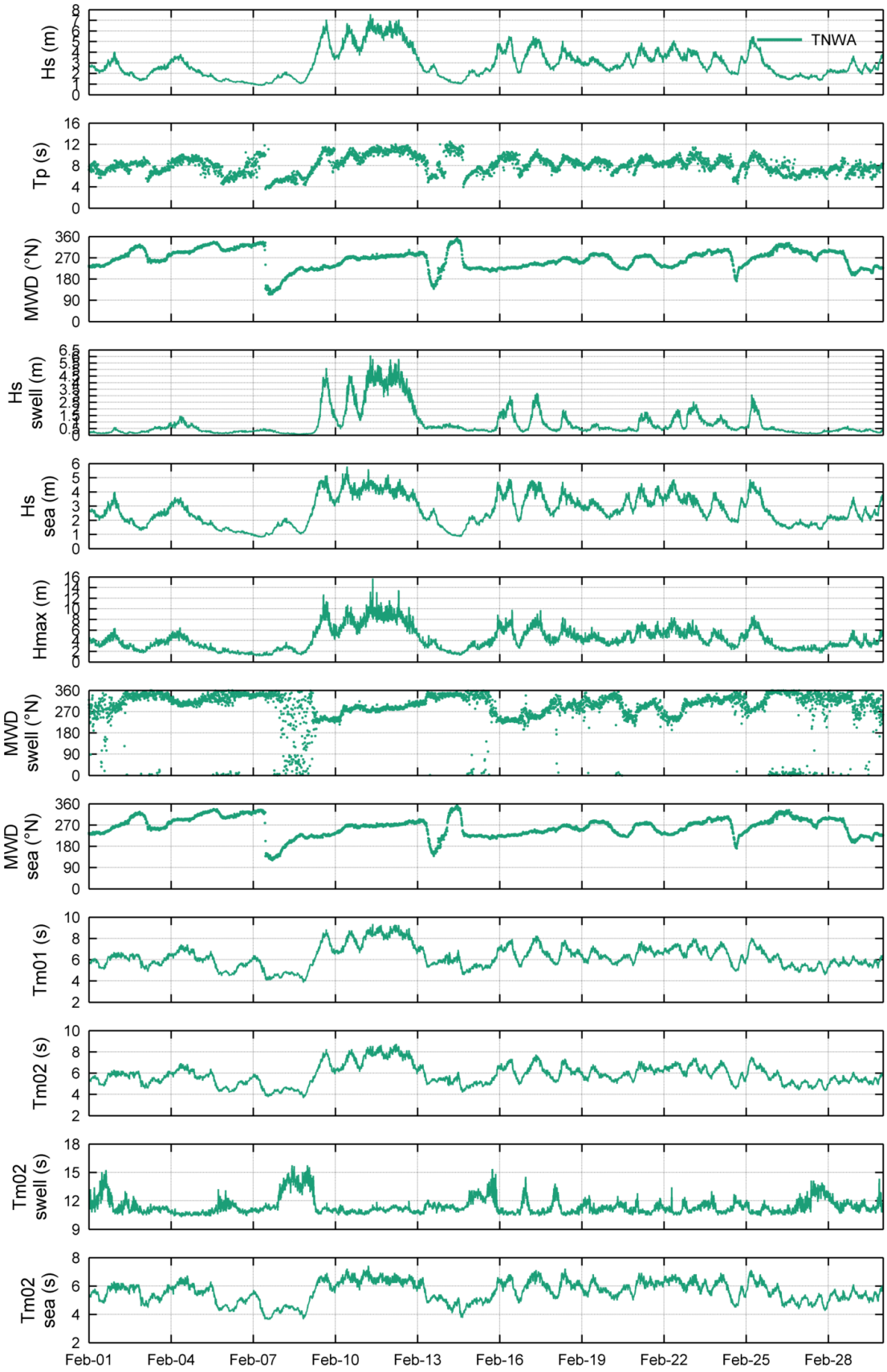


***Figure 4.1:*** *Wave parameters at TNWA (data from February 2020).*

## 4.2 Validation

An overview of the comparisons is first presented, followed by a detailed comparison between the data from TNWA (Section 4.2.2) a with the fixed observations.

### 4.2.1 Overview

Figure 4.2 and Figure 4.3 show the significant wave height and peak wave period roses, respectively, at TNWA and SON. No roses are shown for F161 and F3 because there are no wave direction observations available from these platforms. The roses show, when considering their locations, an overall agreement. Given its location nearer the shore (cf. Figure 1.2), waves from Southwest at TNWA have a more northern alignment at SON.

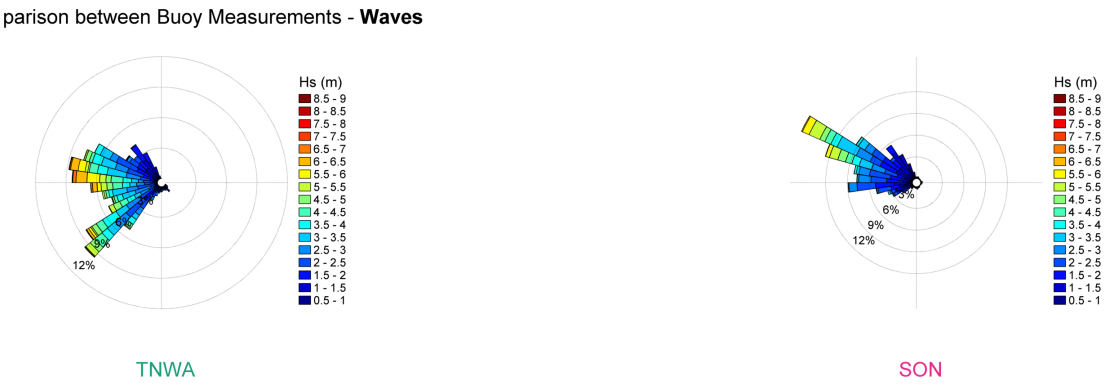


***Figure 4.2:*** *Significant wave height roses (data from February 2020).*

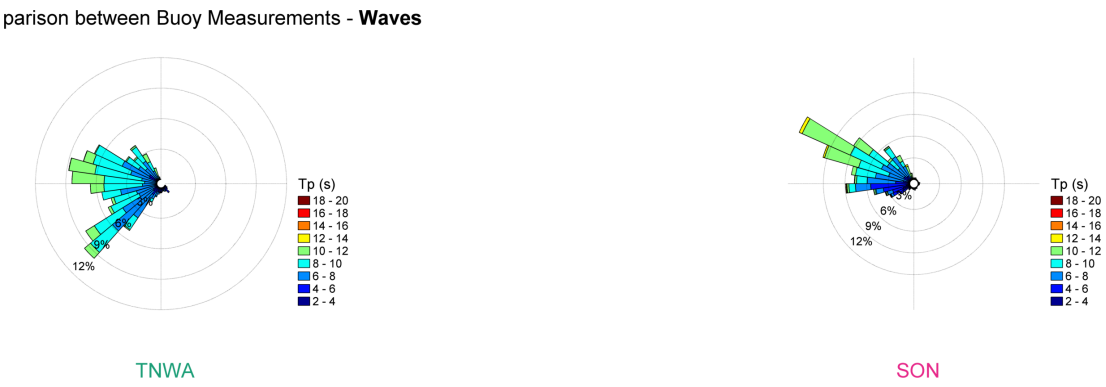


***Figure 4.3:*** *Peak wave period roses (data from February 2020).*

### 4.2.2 Comparisons

Figure 4.4, Figure 4.5 and Figure 4.6 show comparisons between TNWA observations and those at F161, F3 and SON of $H_s$, $T_p$, mean wave period, $T_{m0,2}$, and mean wave direction, $MWD$ (only SON, Figure 4.6). The correlation, root-mean-square error and bias statistics are printed in each of the figures.

As can be seen in the figures, the comparisons between TNWA observations and those:

- at F161 and F3 are excellent in terms of significant and swell wave height and mean wave period and reasonable in terms of peak wave period; and
- at SON are excellent in terms of swell wave height, good in terms of significant wave height and mean wave period, reasonable in terms of mean wave direction and poor in terms of peak wave period.

Discrepancies between the mean wave direction at TNW and SON are expected given the shallower and closer to the shore location of SON (cf. Figure 1.2). Discrepancies in terms of peak wave period between the data from all locations are also expected given the discrete characteristics of the variable.

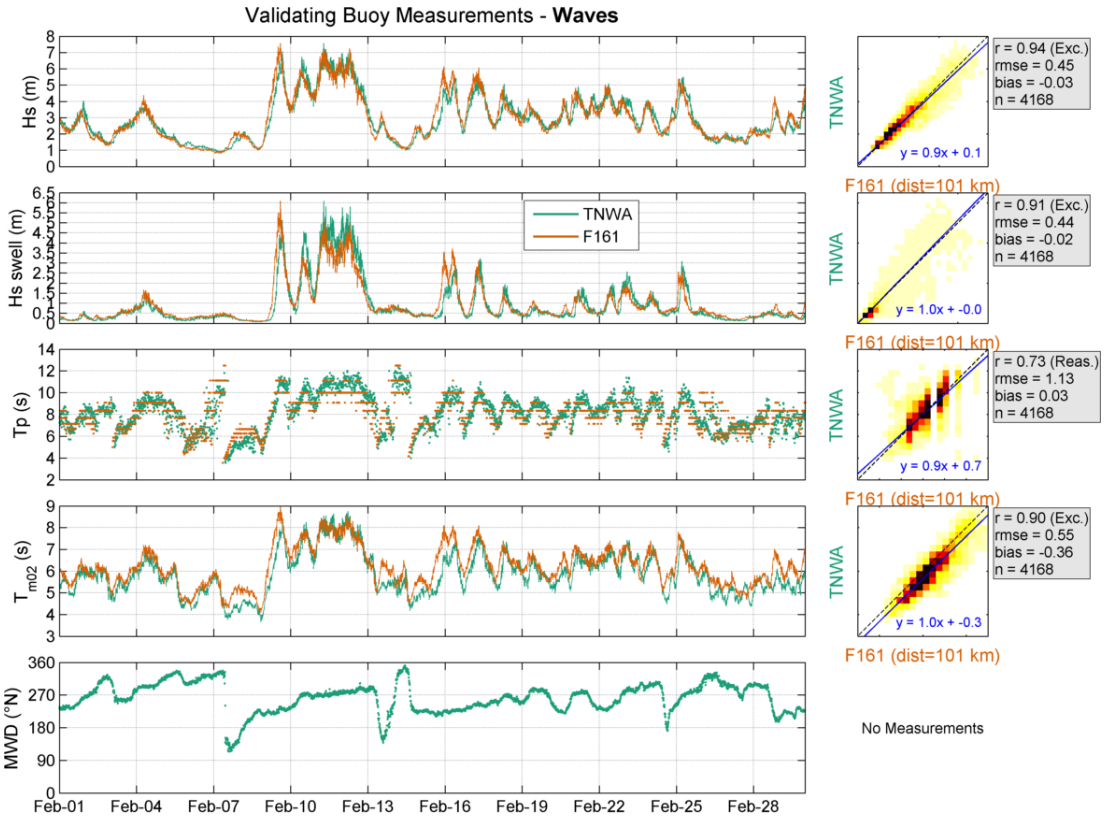


***Figure 4.4:*** *Validation of TNWA (data from February 2020) with F161 wave data. Left panel: Timeseries. Middle panel: Density scatter, with the darker colours indicating more data density.*

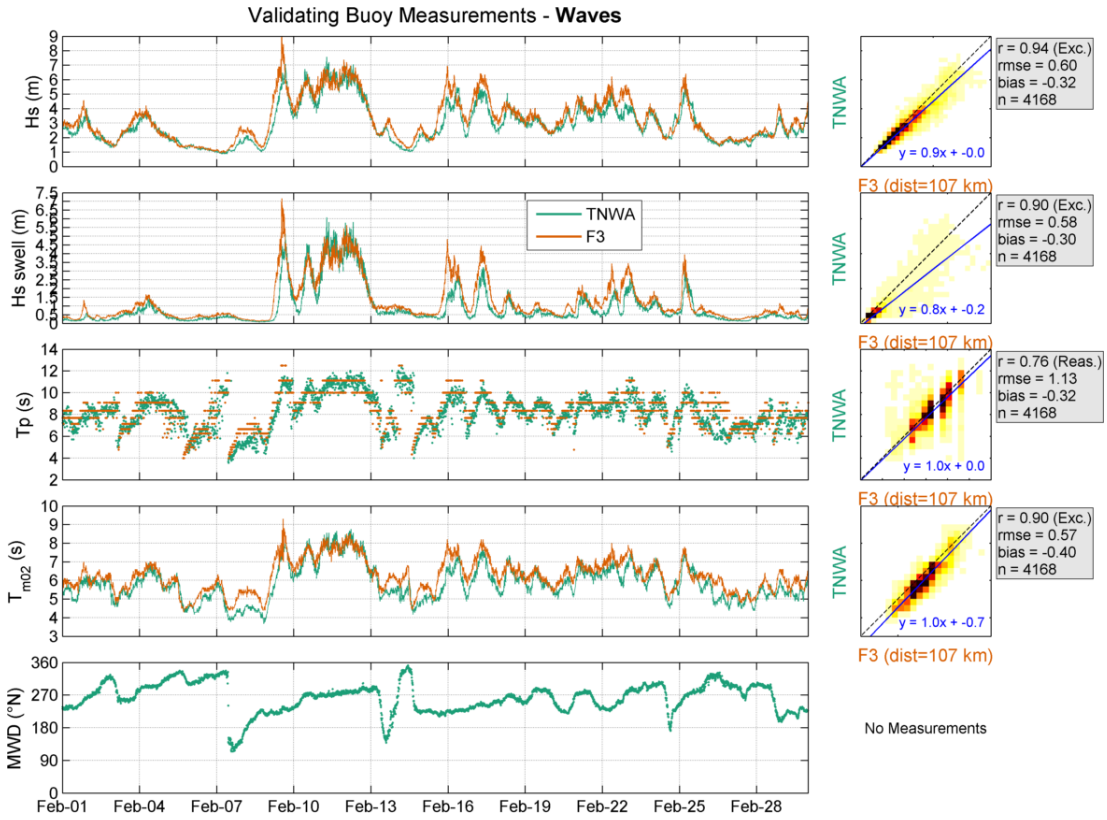


***Figure 4.5:*** *Validation of TNWA (data from February 2020) with F3 wave data. Left panel: Timeseries. Middle panel: Density scatter, with the darker colours indicating more data density.*

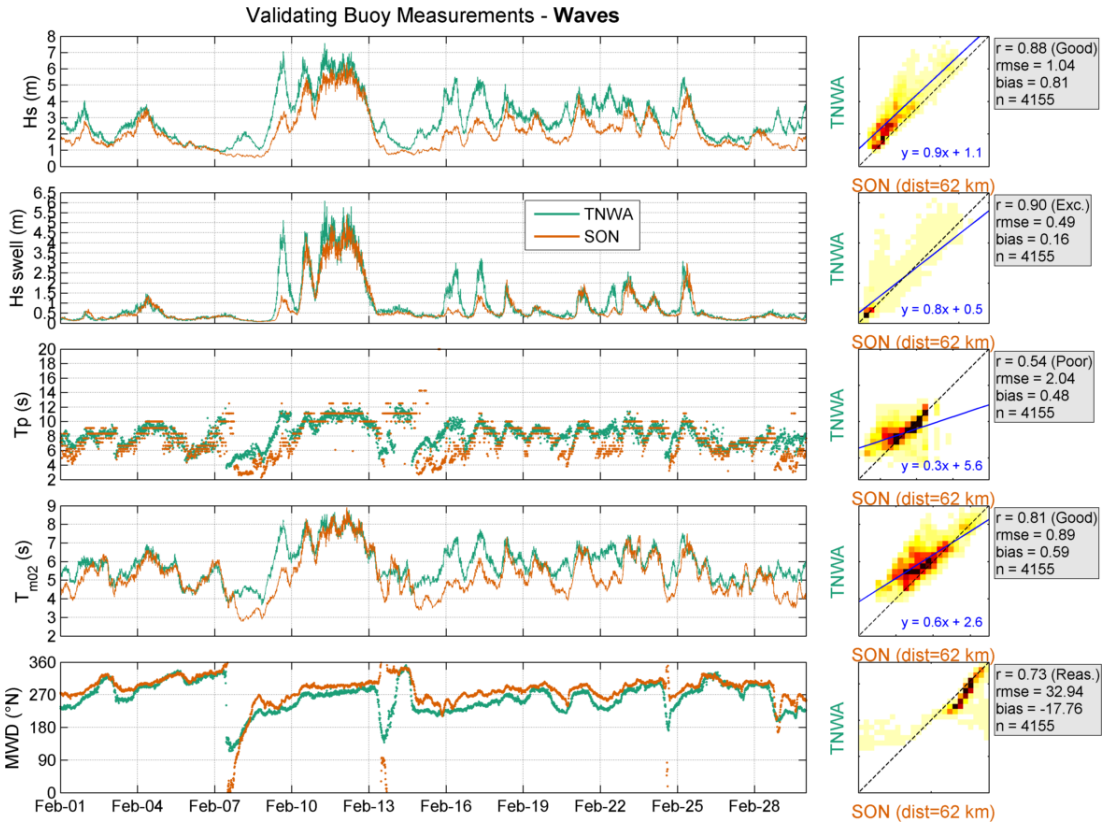


***Figure 4.6:*** *Validation of TNWA (data from February 2020) with SON wave data. Left panel: Timeseries. Middle panel: Density scatter, with the darker colours indicating more data density.*

## 4.3 Summary and conclusions

The correlations between the buoy and the fixed station wave observations given in figures 4.4 to 4.6 are summarized in Table 4.1.

***Table 4.1:*** *Statistical comparison between the TNWA buoy observations and those from the fixed stations.*

| | **TNWA** | | |
|---|---|---|---|
| **Station** | F161 | F3 | SON |
| $H_s$ $r$ **(-)** | 0.94 | 0.94 | 0.88 |
| $H_s$ $n$ **(-)** | 4168 | 4168 | 4155 |
| $H_{sswell}$ $r$ **(-)** | 0.91 | 0.90 | 0.90 |
| $H_{sswell}$ $n$ **(-)** | 4168 | 4168 | 4155 |
| $T_p$ $r$ **(-)** | 0.73 | 0.76 | 0.54 |
| $T_p$ $n$ **(-)** | 4168 | 4168 | 4155 |
| $T_{m02}$ $r$ **(-)** | 0.90 | 0.90 | 0.81 |
| $T_{m02}$ $n$ **(-)** | 4168 | 4168 | 4155 |
| $MWD$ $r$ **(-)** | - | - | 0.73 |
| $MWD$ $n$ **(-)** | - | - | 4155 |

Based on the validation of the data against the platform observations, in which mismatches can be explained by local effects and the discreteness of the wave spectra, it can be concluded that the accuracy of the TNWA buoy wave data is high.

# 5 Temperature

During this deployment period there are only air and surface water temperatures available from TNWA; water temperature data during the whole month and the air temperature data until the 9th of February (cf. Figure 2.1).

## 5.1 Ten Noorden van de Waddeneilanden description

Figure 5.1 shows the at TNWA observed air and water temperature and their differences.

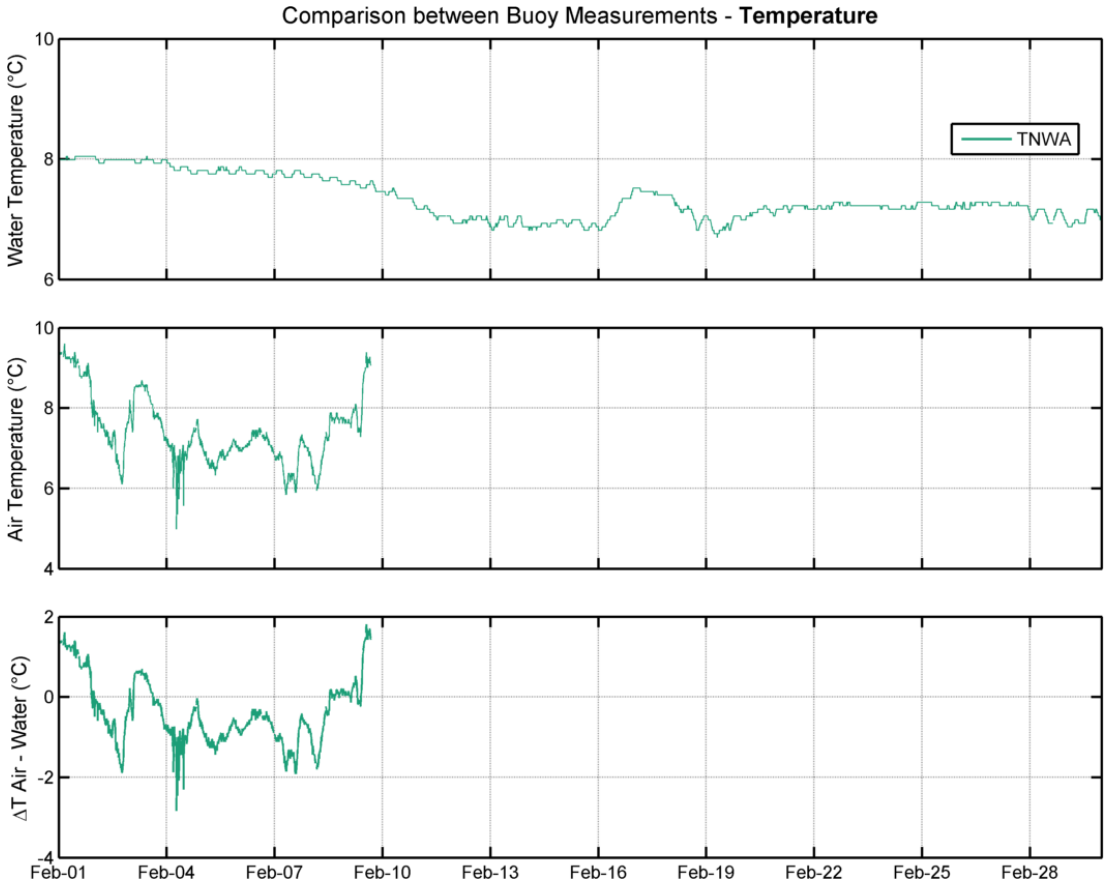


***Figure 5.1:*** *Temperature difference measured at LiDAR buoys (data from February 2020).*

## 5.2 Validation

The comparisons between fixed station measurements and the TNWA data are presented in Section 5.2.1 (water temperature) and in Section 5.2.2 (air temperature).

### 5.2.1 Water Temperature

A timeseries comparison between the observations from TNWA and the fixed stations is presented in Figure 5.2. The water temperature observations from the fixed stations are all surface temperatures. Figure 5.2 shows that large spatial variations in the temperature during this month, with the highest temperatures being observed at the start of the month at TNWA and during the second half of the month at K13.

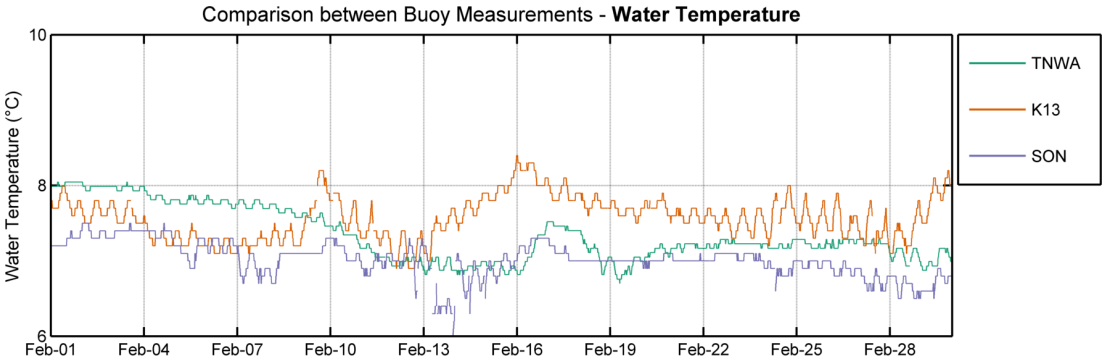


***Figure 5.2:*** *Water temperature measurements from all locations (data from February 2020).*

A direct comparison of the measured surface water temperature at TNWA against the fixed stations is provided in Figure 5.3 . As could already be inferred from the spatial variations shown in Figure 5.2, the agreements are all poor.

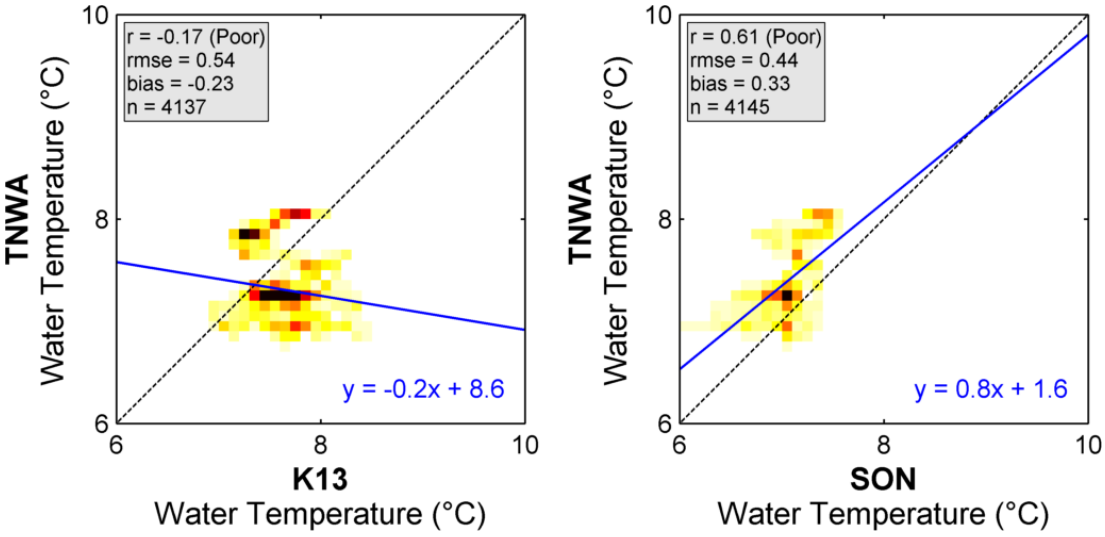


***Figure 5.3:*** *Surface water temperature comparison at TNWA (data from February 2020).*

### 5.2.2 Air Temperature

A timeseries comparison of the measured air temperature between the observations at TNWA and those at BG is provided in Figure 5.4. In the periods when the data overlap (until the 9$^{th}$), the data are aligned and in good agreement as can be also be seen in Figure 5.5. Note that the stepwise timeseries of BG is due to the coarse (1 °C) discretization of the available raw measurements.

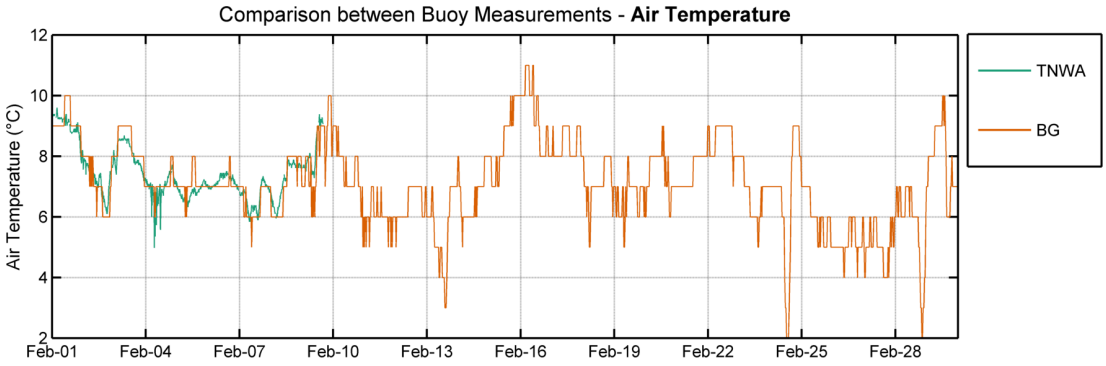


***Figure 5.4:*** *Air temperature measurements from all locations (data from February 2020).*

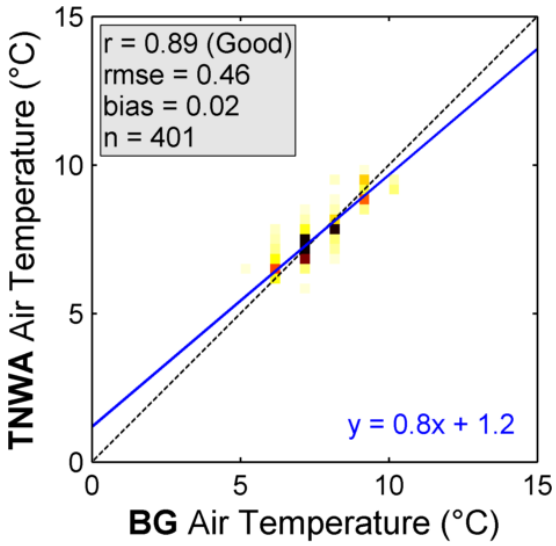


***Figure 5.5:*** *Air temperature comparison at TNWA (data from February 2020).*

## 5.3 Conclusions

The validation of the water temperature data shows large spatial variations, leading to poor agreements between the data. On the other hand, there is a good agreement between the TNWA observed air temperatures and those from the nearby BG station.

# 6 Air Pressure

## 6.1 Overview

An overview of the available air pressure measurements (TNWA, L91, F161, K13, and F3) is shown in Figure 6.1. The signals show near-identical variations in time, as expected, given their proximity with respect to macro-atmospheric forcings, and a spatial gradient during most of the time with the higher values L91 and low values at F3.

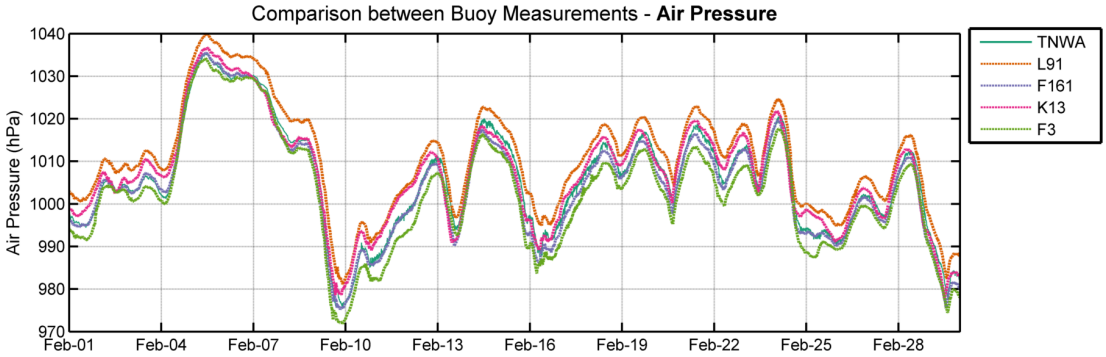


***Figure 6.1:*** *Air pressure measurements from all locations.*

## 6.2 Validation

A direct comparison of the measured air pressure at TNWA against those of the fixed stations is given in Figure 6.2. As could already be inferred from the variations shown in Figure 6.1, in spite of the biases due to the observed spatial gradients, the agreements are all excellent.

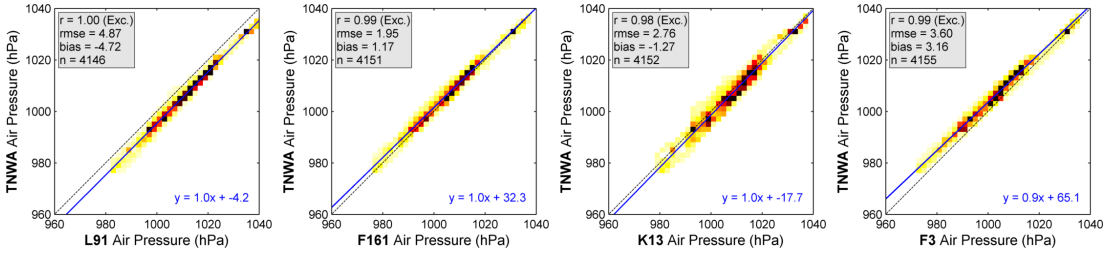


***Figure 6.2:*** *Air pressure comparison at TNWA (data from February 2020).*

## 6.3 Conclusions

The validation of the air pressure data shows, as expected given their proximity in terms of macro-atmospheric forcings, an excellent agreement between the TNWA observations and those from the fixed stations.

# 7 Currents

## 7.1 Ten Noorden van de Waddeneilanden description

During this period the current speed and direction are measured at depths 3 to 38 m with a spacing of 1 m at TNWA. Given that the observations close to the bottom are of lower quality and not always available due to the water level variations, in this report we only consider the current velocity data down to a depth of 33 m.

To get a full overview of the data a movie was created with the time evolution of vertical current profiles at TNWA (see here).

Figure 7.1 shows the timeseries of the observed surface (3 m) current speeds, with the corresponding roses being given in Figure 7.2. Figure 7.3 shows the observed current speeds and directions as a function of depth. As can be seen in the figure, the currents in TNW are predominantly tidally driven, with an alignment close to East-West and with the stronger currents being towards the East.

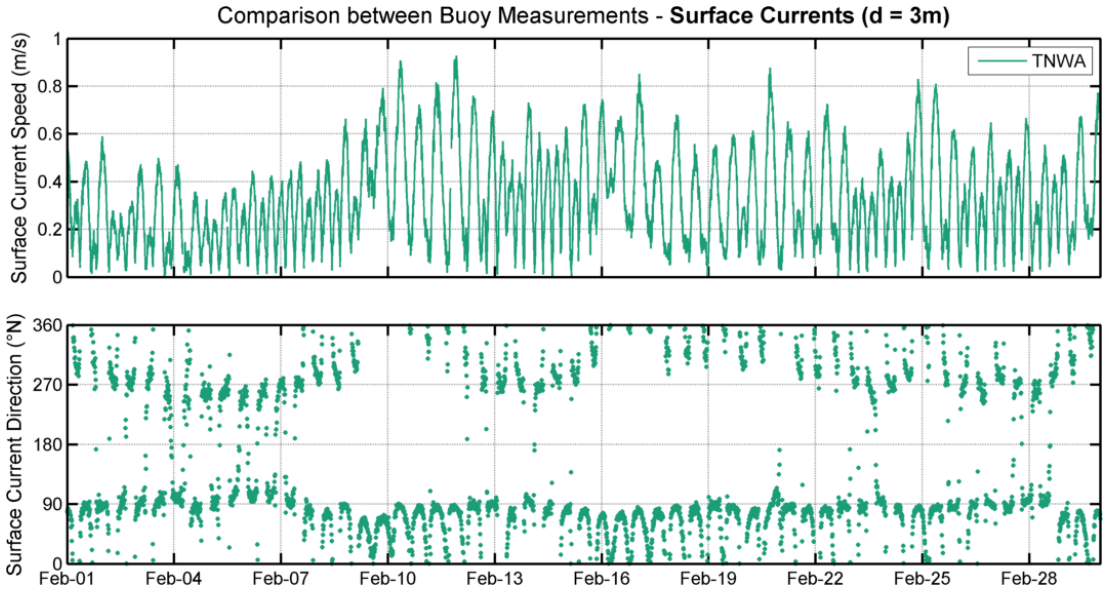


***Figure 7.1:*** *Surface currents at each buoy. Left panels: Timeseries. The oceanographic convention is used for the current directions, so all current directions are going to, clockwise from North.*

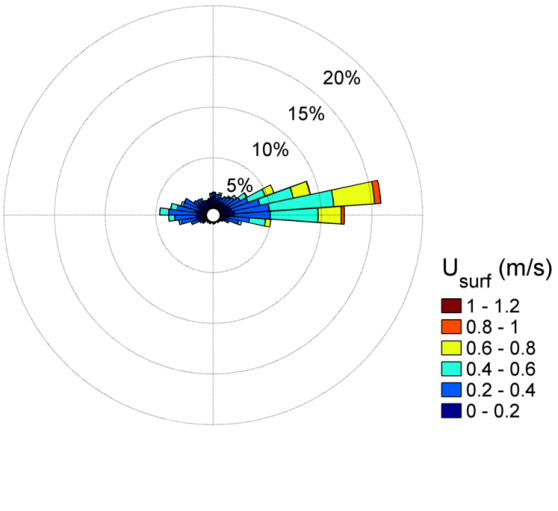


***Figure 7.2:*** *Surface (3 m) current rose (bin width 8°) at TNWA (data from February 2020). The current direction is the direction the piles point to away from the centre of the rose.*

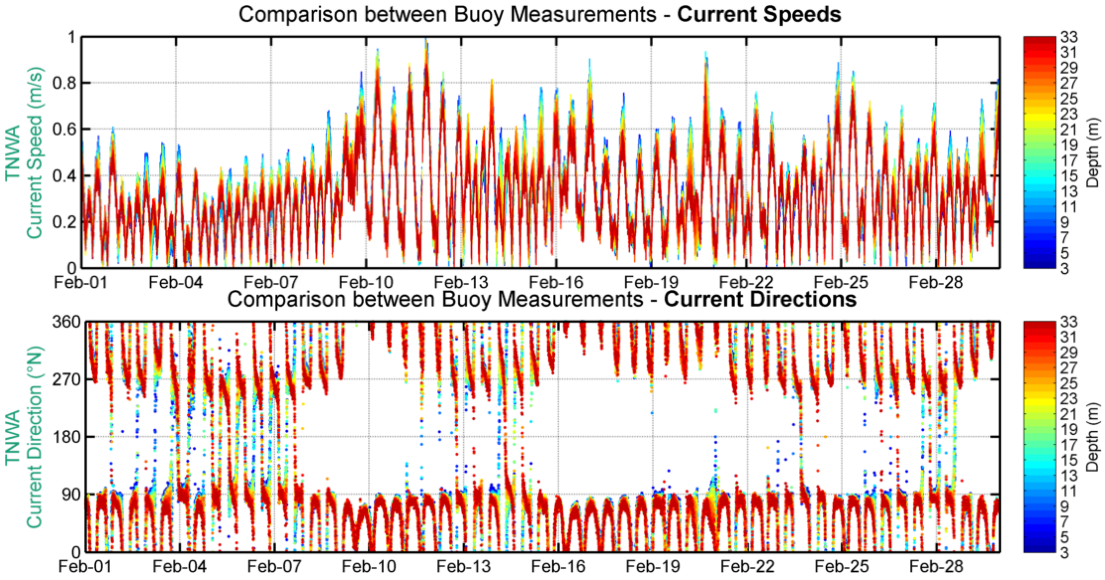


***Figure 7.3:*** *Current speed and direction (by depth) at TNWA. The oceanographic convention is used for the current directions, so all current directions are going to clockwise from North.*

Figure 7.4 shows all observed vertical current profiles (grey lines) and the mean profile (red line). Note that, due to the water level variations, the distance between the deepest measuring level and the bottom varies and this leads to a less reliable description of the profile close to the bed using the relative current velocity approach we have applied to compute the profile. Nevertheless, the shown mean profile of TNWA observations appears realistic and shows, as could already be seen in the figures above, a small average increase in the current from the surface down to a depth of 6 m and a decrease downwards from that depth.

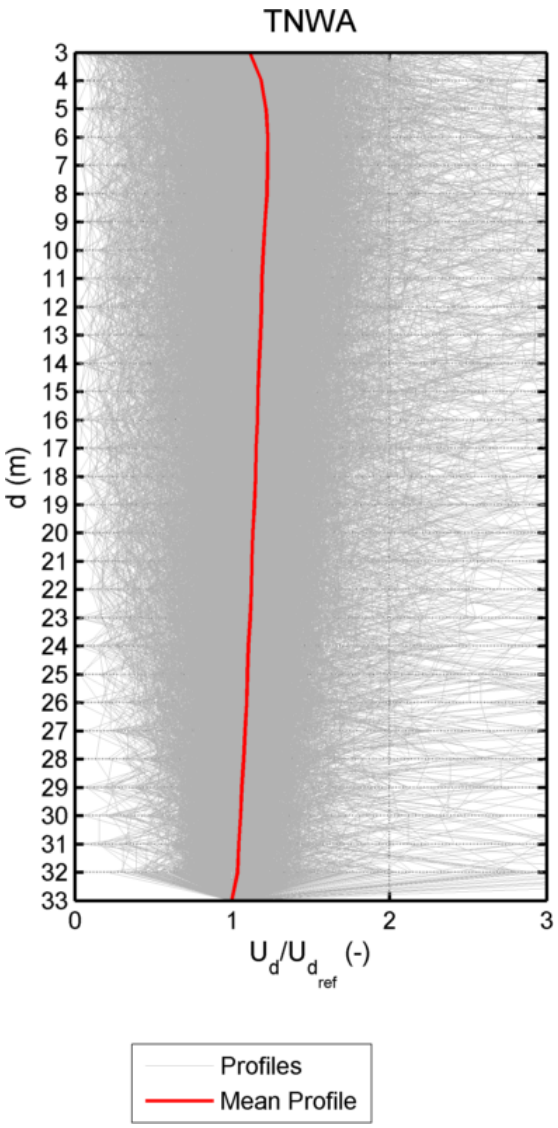


***Figure 7.4:*** *Normalized current speed vertical profiles (from February 2020). The x-axis has a fixed lower limit of 0 and upper limit of 3 for readability.*

## 7.2 Validation

The validation of the measured TNWA currents is completed with data from Deltares 3D Dutch Continental Shelf Model-Flexible Mesh (3D DCSM-FM) described in the following and which has been run purposely for this validation.

### 7.2.1 Model description

3D DCSM-FM covers the northwest European continental shelf, specifically the area between 15°W to 13°E and 43°N to 64°N, and includes the North Sea and adjacent shallow seas and estuaries such as the Wadden Sea and the Eastern and Western Scheldt. It is loosely based on the two-dimensional operational water level forecasting models of the Netherlands (Zijl *et al.* 2013, 2015), but uses a flexible mesh with resolution increasing with decreasing water depth (Figure 7.5). The smallest cells have a size of 2/3‘ in east-west direction and 1/2‘ in north-south direction, which corresponds to 840 m by 930 m in Dutch waters. The optimization methodology is similar to (Zijl *et al.*, 2013), but now excludes bathymetry adjustment. The bathymetry is based on data from EMODnet supplemented with survey data for the Dutch coastal zone (cf. Figure 7.6)). 3D DCSM-FM uses 20 equidistant sigma-layer in the vertical and includes temperature and salinity as state parameters. At the lateral open boundaries water levels consisting of a tide and surge component are provided. For the tide 33 harmonic constituents from the global tide model FES2012 were used, while for the surge an Inverse Barometer Correction is applied (Zijl *et al.*, 2013). The model includes river discharges, while meteorological forcing in terms of atmospheric wind, mean level pressure, air temperature, cloud cover and dew point temperature are obtained from the KNMI operational Numerical Weather Prediction model Hirlam7.2. (Zijl and Veenstra, 2018) provides further details on the set-up and validation of 3D DCSM-FM .

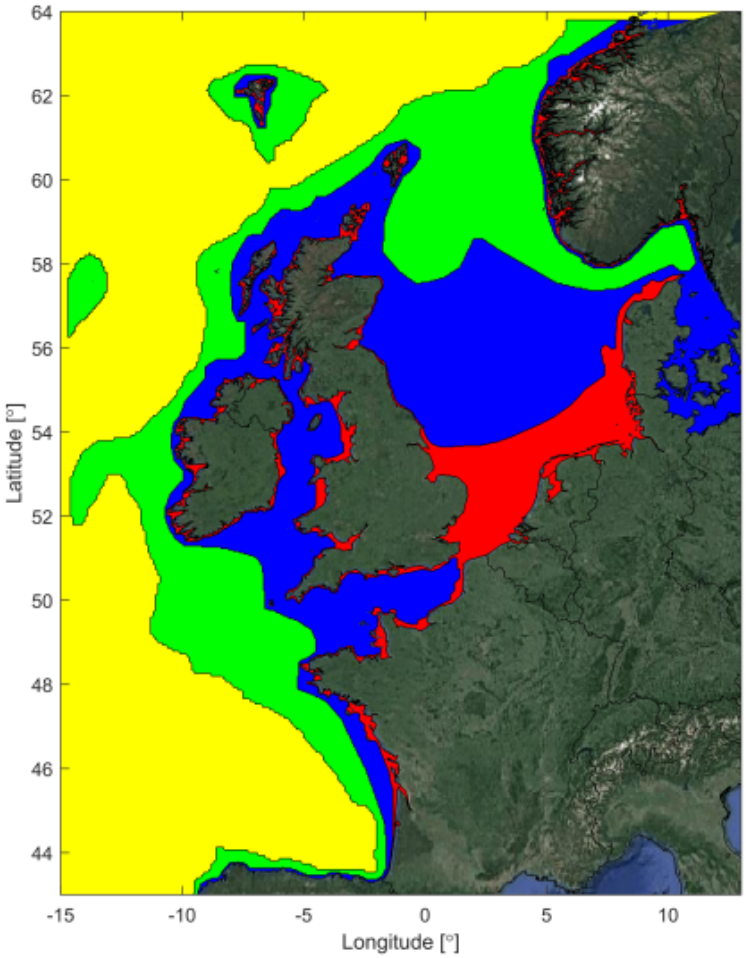


***Figure 7.5:*** *Overview of the 3D DCSM-FM model network with the colors indicating the grid size (yellow: ≈ 4 nm; green: ≈ 2 nm; blue: ≈ 1 nm; red: ≈ 0.5 nm).*

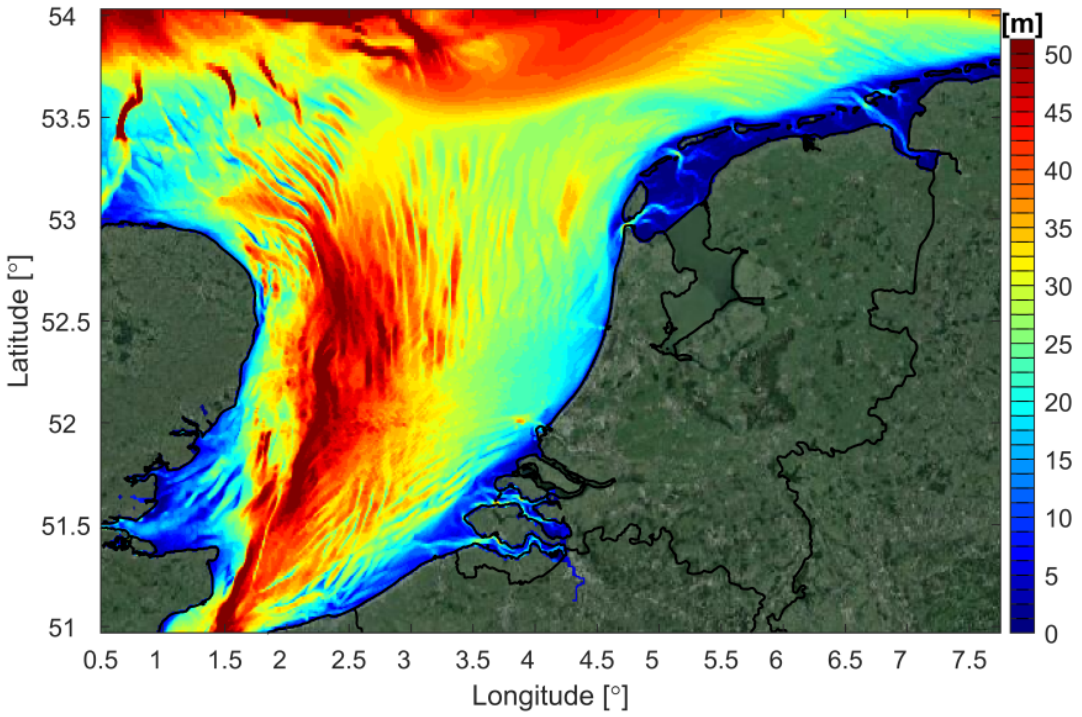


***Figure 7.6:*** *3D DCSM-FM model bathymetry in the southern North Sea (depths relative to MSL; source: EMODnet).*

### 7.2.2 Model results at TNWA

A direct comparison between the 3D DCSM-FM surface current (d = 3 m) at TNWA and the buoy observations is given in Figure 7.7 in terms of timeseries and Figure 7.8 in terms of roses. The same comparisons are shown in Figure 7.9 in terms of timeseries and Figure 7.10 in terms of roses for the current at 23 m (about 60% down the water column). At the surface level the agreements are excellent in terms of current speed and reasonable in terms of current direction and at the 23 m level the agreements are good in terms of current speed and also reasonable in terms of current direction. Furthermore, the roses show more directional spreading in the observations and a larger west-east current asymmetry, with a higher predominance of currents towards the East in the observations. Table 7.1 shows the error statistics between the current speed and direction of the model at TNWA and the TNWA data at the observed levels from a depth of 3 m to 33 m. In terms of current speed the agreements are reasonable to excellent. In terms of current direction the agreements are reasonable at all levels. The lower current direction correlations can to a large extent be explained by the nature and variability of the current direction signal. Due to the rotating nature of the currents, especially when they rapidly rotate towards offshore (directions close to 350) the timing of the observations can be off. This occurs, however, during short time periods and mostly when the current speeds are low.

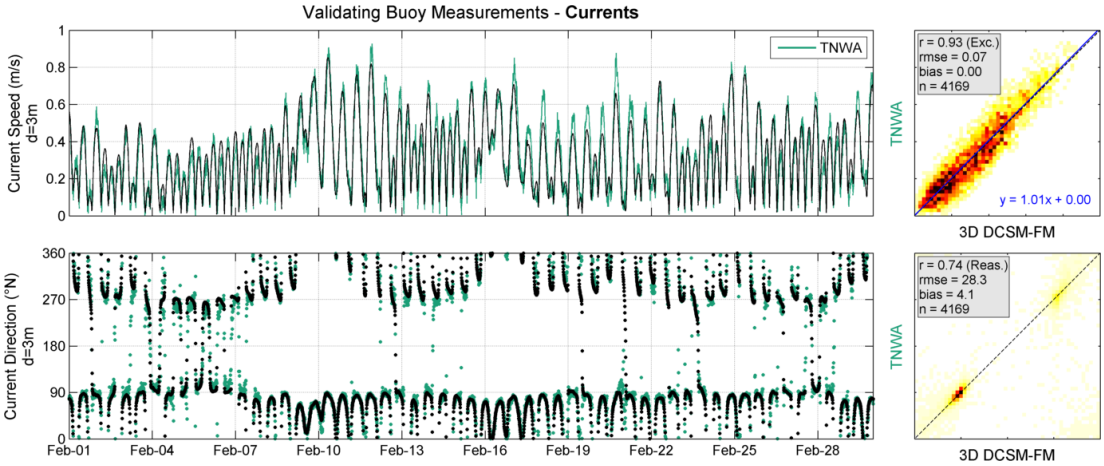


***Figure 7.7:*** *Surface (d=3 m) current comparison at TNWA (data from February 2020).*

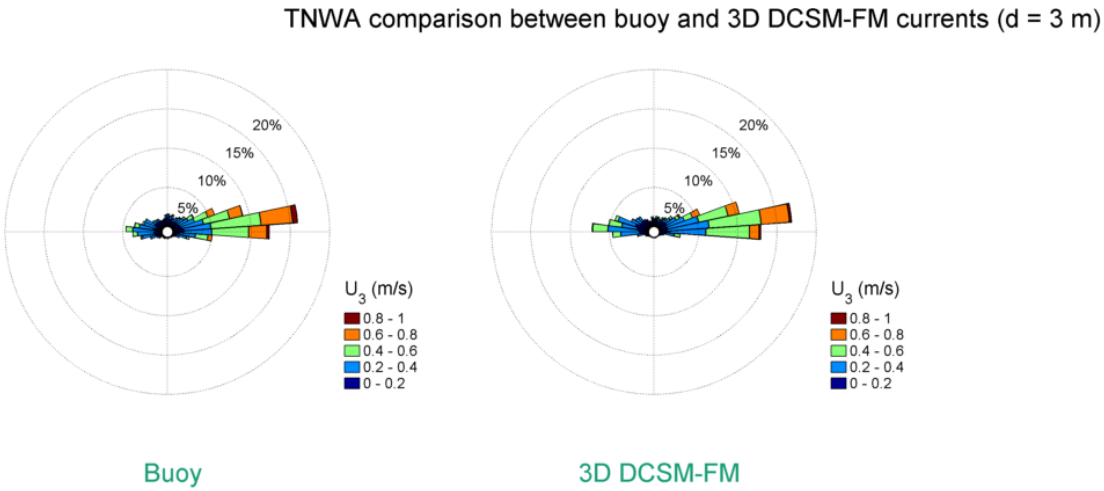


***Figure 7.8:*** *Buoy and 3D DCSM-FM roses (bin width 8°) of the surface (3 m) current velocity at TNWA (data from February 2020. The current direction is the direction the piles point to away from the centre of the rose.*

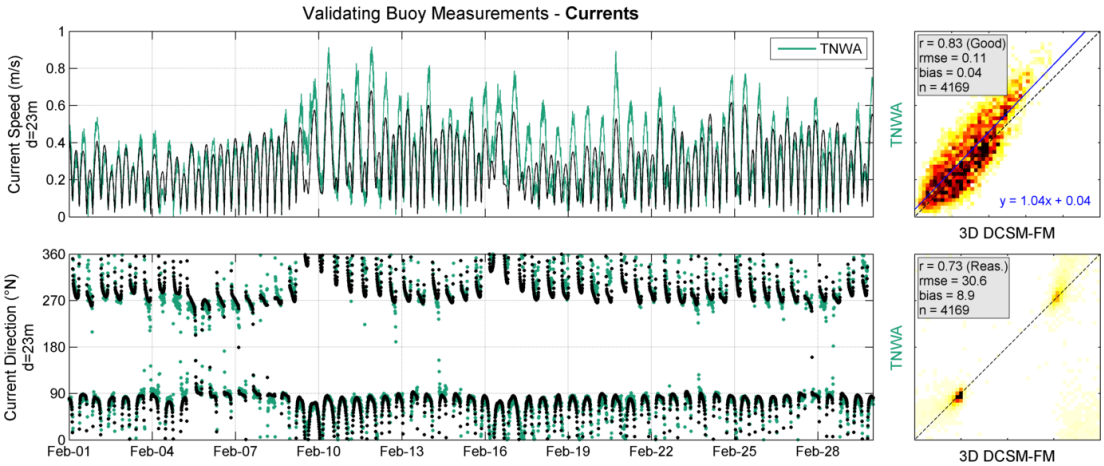


***Figure 7.9:*** *Current comparison at depth of 23 m TNWA (data from February 2020.*

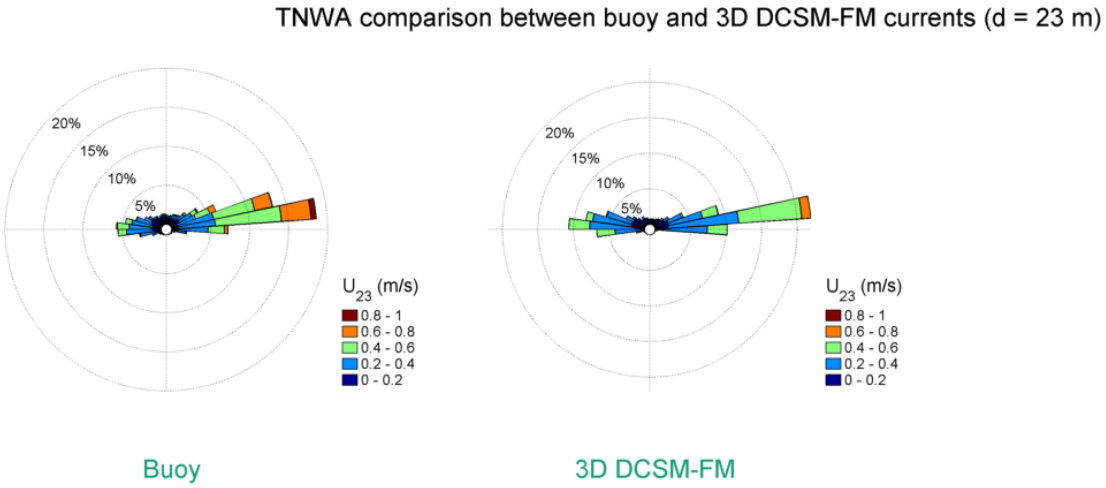


***Figure 7.10:*** *Buoy and 3D DCSM-FM roses (bin width 8°) of the 23 m current velocity at TNWA (data from February 2020). The current direction is the direction the piles point to away from the centre of the rose.*

***Table 7.1:*** *Statistical comparison between the 3D DCSM-FM results with TNWA with depth.*

| | Current Speed | | | | Current Direction | | |
|---|---|---|---|---|---|---|---|
| **Depth (m)** | $r$ **(-)** | **Bias (m/s)** | **Symm. Slope (-)** | $n$ **(-)** | $r$ **(-)** | **Bias (°)** | $n$ **(-)** |
| 3 | 0.93 | 0.00 | 1.02 | 4169 | 0.74 | 4.1 | 4169 |
| 4 | 0.92 | 0.03 | 1.10 | 4169 | 0.75 | 4.2 | 4169 |
| 5 | 0.91 | 0.04 | 1.12 | 4169 | 0.75 | 5.1 | 4169 |
| 6 | 0.90 | 0.04 | 1.14 | 4169 | 0.74 | 6.2 | 4169 |
| 7 | 0.90 | 0.04 | 1.15 | 4169 | 0.73 | 6.0 | 4169 |
| 8 | 0.89 | 0.05 | 1.15 | 4169 | 0.72 | 6.9 | 4169 |
| 9 | 0.88 | 0.04 | 1.16 | 4169 | 0.72 | 6.8 | 4169 |
| 10 | 0.87 | 0.04 | 1.16 | 4169 | 0.71 | 7.3 | 4169 |
| 11 | 0.86 | 0.04 | 1.16 | 4169 | 0.71 | 7.1 | 4169 |
| 12 | 0.87 | 0.04 | 1.16 | 4169 | 0.70 | 6.8 | 4169 |
| 13 | 0.87 | 0.04 | 1.17 | 4169 | 0.71 | 7.2 | 4169 |
| 14 | 0.87 | 0.04 | 1.17 | 4169 | 0.70 | 7.4 | 4169 |
| 15 | 0.86 | 0.04 | 1.17 | 4169 | 0.71 | 7.5 | 4169 |
| 16 | 0.86 | 0.04 | 1.17 | 4169 | 0.71 | 7.4 | 4169 |
| 17 | 0.85 | 0.04 | 1.17 | 4168 | 0.70 | 7.8 | 4168 |
| 18 | 0.85 | 0.04 | 1.17 | 4169 | 0.71 | 8.3 | 4169 |
| 19 | 0.85 | 0.04 | 1.18 | 4169 | 0.71 | 8.3 | 4169 |
| 20 | 0.84 | 0.04 | 1.17 | 4168 | 0.72 | 8.9 | 4168 |
| 21 | 0.83 | 0.04 | 1.17 | 4169 | 0.72 | 8.7 | 4169 |
| 22 | 0.84 | 0.04 | 1.17 | 4169 | 0.73 | 8.9 | 4169 |
| 23 | 0.83 | 0.04 | 1.17 | 4169 | 0.73 | 8.9 | 4169 |
| 24 | 0.83 | 0.04 | 1.17 | 4169 | 0.74 | 9.2 | 4169 |
| 25 | 0.82 | 0.04 | 1.17 | 4169 | 0.74 | 9.1 | 4169 |
| 26 | 0.82 | 0.04 | 1.16 | 4169 | 0.74 | 9.2 | 4169 |
| 27 | 0.81 | 0.04 | 1.16 | 4169 | 0.75 | 9.5 | 4169 |
| 28 | 0.82 | 0.04 | 1.15 | 4168 | 0.75 | 8.9 | 4168 |
| 29 | 0.81 | 0.04 | 1.16 | 4169 | 0.74 | 9.3 | 4169 |
| 30 | 0.80 | 0.03 | 1.14 | 4169 | 0.74 | 8.8 | 4169 |
| 31 | 0.79 | 0.04 | 1.15 | 4169 | 0.73 | 8.8 | 4169 |
| 32 | 0.79 | 0.03 | 1.13 | 4169 | 0.73 | 8.3 | 4169 |
| 33 | 0.78 | 0.03 | 1.15 | 4169 | 0.72 | 8.4 | 4169 |

## 7.3 Conclusions

As shown above, the agreement between the current speed observations from TNWA with model results is high. The obtained relatively lower correlations in the current direction are not considered to be due to lack of accuracy in the current direction observations, but model resolution effects and the effect of the nature and variability of the current direction signal on the buoy observations. The found general agreement between the buoy and model data, testify the quality of both the model results and the observations.

## References

Fisher, N. I., 1993. *Statistical analysis of circular data*. Cambridge Univ. Press.

Fisher, N. I. and A. J. Lee, 1983. "A correlation coefficient for circular data." *Biometrika* 70: 327–332.

KNMI, 2009. *HiRLAM version H7.2*. Tech. Rep. http://projects.knmi.nl/datacentrum/catalogus/catalogus/content/history/HIRLAM72_eng__151009.pdf, KNMI.

Wieringa, J. and P. Rijkoort, 1983. *Windklimaat van Nederland (in Dutch)*. KNMI (staatsuitgeverij).

Zijl, F., J. Sumihar and M. Verlaan, 2015. "Application of data assimilation for improved operational water level forecasting on the northwest European shelf and North Sea." *Ocean Dynamics* 65 (11).

Zijl, F. and J. Veenstra, 2018. *Setup and validation of 3D DCSM-FM*. Deltares memo 1220339-005-zks-0003.

Zijl, F., M. Verlaan and H. Gerritsen, 2013. "Improved water-level forecasting for the Northwest European Shelf and North Sea through direct modelling of tide, surge and non-linear interaction." *Ocean Dynamics* 63 (7).